

Review article



The seas around China in a warming climate

Fan Wang ^{1,2}✉, Xuegang Li ^{1,2}, Xiaohui Tang ^{1,2}, Xiaoxia Sun ^{1,2}, Junlong Zhang ^{1,2}, Dezhou Yang ^{1,2}, Lingjing Xu ¹, Hui Zhang ^{1,2}, Huamao Yuan ^{1,2}, Yuntao Wang ³, Yulong Yao ^{4,5}, Chunzai Wang ^{4,5}, Yaru Guo ¹, Qiuping Ren ¹, Yuanlong Li ^{1,2}✉, Rongwang Zhang ^{4,5}, Xin Wang ^{4,5}, Bin Zhang ¹ & Zhongli Sha ^{1,2}

Abstract

Anthropogenic forcings have led to multifaceted changes in the seas around China, which include the Bohai, Yellow, East China and South China Seas, affecting the functions and services they provide. In this Review, we synthesize physical, biogeochemical and biological findings to understand how the seas around China have changed and are projected to change under a warming climate. The average surface temperature of these seas increased by $0.10\text{--}0.14\text{ }^{\circ}\text{C dec}^{-1}$ over 1950–2021. Meanwhile, the annual frequency and average intensity of marine heatwaves increased by $1\text{--}2\text{ dec}^{-1}$ and $0.1\text{--}0.3\text{ }^{\circ}\text{C dec}^{-1}$ since the 1980s, respectively. Terrestrial input has increased nutrient concentrations and composition changes in coastal waters. These warming and nutrient changes have increased the severity of hypoxia and acidification, leading to complex changes in primary productivity. Changes to marine organisms such as plankton, benthos and fish are also apparent, including the northward invasion of warm-water species and miniaturization. These observed changes are projected to persist into the future. These coupled physical–ecological changes highlight the need for strengthened multidisciplinary oceanographic research in the seas around China.

Sections

Introduction

Historical physical changes

Historical biogeochemical changes

Historical biological changes

Projected changes

Summary and future perspectives

¹Institute of Oceanology, Chinese Academy of Sciences, Qingdao, China. ²Laoshan Laboratory, Qingdao, China.

³State Key Laboratory of Satellite Ocean Environment Dynamics, Second Institute of Oceanography, Ministry of Natural Resources, Hangzhou, China. ⁴State Key Laboratory of Tropical Oceanography, South China Sea Institute of Oceanology, Chinese Academy of Sciences, Guangzhou, China. ⁵Global Ocean and Climate Research Center, South China Sea Institute of Oceanology, Chinese Academy of Sciences, Guangzhou, China. ✉e-mail: fwang@qdio.ac.cn; liyuanlong@qdio.ac.cn

Introduction

The seas around China (SAC; Supplementary Table 1) collectively refer to the Bohai Sea (BS), Yellow Sea (YS), East China Sea (ECS) and South China Sea (SCS). Billions of people residing in East and Southeast Asia rely on the functions, goods and services provided by these seas, including fisheries, aquaculture, shipping, water resource, tourism and recreation. For example, in 2019, total fisheries production in the SAC reached 19.2 million tonnes¹, providing jobs for more than 10 million people. In addition, the temperatures of the SAC regulate the climate and weather of surrounding countries, typically by modulating behaviours of the monsoon and typhoons².

Observations indicate a range of coupled physical–ecological changes to the SAC, including ocean temperature^{4–6} and circulation^{7–10}, biogeochemical properties^{11–17}, primary productivity^{18–20} and marine biodiversity^{14,21–24}. Indeed, widespread warming is apparent throughout the SAC, albeit with spatial and seasonal variability^{4–6,25}, accompanied by increased frequency and intensity of marine heatwaves^{26–29}. Corresponding changes to ocean stratification, coupled with enhanced nutrient inputs from land-based human activities, have further increased the severity and frequency of hypoxia and acidification^{11–14,30,31}. These physical and biogeochemical changes, in turn, influence biological systems, leading to a northward expansion of warm-water species and a miniaturization trend in plankton^{21,32,33}, benthos^{34,35} and fish^{36,37}, affecting the functioning of ecosystems through perturbed trophic webs.

These observed changes, which are likely to continue in the future, have wide-ranging socioeconomic impacts. For example, the 2017 marine heatwaves that occurred in the ECS led to harmful algal blooms and mass mortalities of farmed fish^{26,38,39}. As such, it is vital to understand the coupled changes across the SAC, both observed and projected, to inform adaptation plans and minimize their impacts. By pinpointing research priorities and integrating research efforts to better support prediction and risk evaluation, this effort would benefit a broad range of scientific disciplines, policymakers and the public.

In this Review, we outline the historical and projected effects of a warming climate on the SAC. We begin by outlining changes in the physical system, including changes in sea surface temperature (SST), marine heatwaves and ocean circulation. We next discuss biogeochemical properties, focusing on nutrients, hypoxia, acidification and carbon uptake. Resultant ecological changes are subsequently detailed, incorporating alterations to plankton and benthic communities as well as fisheries. Projections for these systems are discussed next, before ending with recommendations for future research.

Historical physical changes

Physical changes in the SAC underlie many subsequent ecological and biogeochemical changes. Observed physical changes since the mid-twentieth century are now discussed, focusing on SST, marine heatwaves and ocean circulation.

Ocean warming

Rising ocean temperatures have been observed in most parts of the SAC in response to anthropogenic greenhouse warming, albeit with marked spatiotemporal variability (Fig. 1) and dataset dependence (Supplementary Table 3). Averaged across the SAC, SST warming reached $0.10\text{--}0.14\text{ }^{\circ}\text{C dec}^{-1}$ during 1950–2021 and accelerated to $0.14\text{--}0.16\text{ }^{\circ}\text{C dec}^{-1}$ over 1982–2021 (Fig. 1a–c). This warming exceeds that of the global average SST ($0.07\text{--}0.10\text{ }^{\circ}\text{C dec}^{-1}$ during 1950–2021 and $0.09\text{--}0.12\text{ }^{\circ}\text{C dec}^{-1}$ during 1982–2021) (Supplementary Table 2),

owing to the small thermal inertia associated with the shallow depths of the SAC^{40–42} and enhanced heat transport by the Kuroshio current^{7,43}.

Embedded within this longer-term warming trend are substantial interdecadal variations (Fig. 1c). According to the Hadley Centre Sea Ice and Sea Surface Temperature (HadISST⁴⁴) dataset, the SAC warmed by $0.31\text{ }^{\circ}\text{C dec}^{-1}$ over 1979–1998, cooled by $-0.27\text{ }^{\circ}\text{C dec}^{-1}$ during 1998–2011 (corresponding to the slowdown of global surface warming^{45,46}), and warmed by $0.45\text{ }^{\circ}\text{C dec}^{-1}$ over 2011–2019. Phase shifts of the Pacific Decadal Oscillation⁴⁷ (PDO) are believed to be responsible for these interdecadal variations^{13,48,49} via influences on the East Asian monsoon^{50–52} and the Kuroshio current^{43,53}. Specifically, the positive phase of the PDO, as during 1979–1998, induces positive surface pressure anomalies across the northwest Pacific, weakening the winter monsoon over the SAC, enhancing heat advection from the Kuroshio and suppressing latent heat release^{43,48,49,54}. Negative PDO phases generally have the opposite effect, explaining the cooling from 1998 to 2011. Besides the PDO, influences from the Atlantic and Arctic climates have also been proposed to explain interdecadal SST variations of the SAC^{49,55,56}.

Spatial heterogeneity dominates the pattern of SST warming across the SAC (Fig. 1a,b). SST trends are strongest in the ECS^{6,57} (Fig. 1d), reaching $0.19 \pm 0.03\text{ }^{\circ}\text{C dec}^{-1}$ from 1950 to 2021 and $0.23 \pm 0.08\text{ }^{\circ}\text{C dec}^{-1}$ from 1982 to 2021 in HadISST, 2–3 times the global average (Supplementary Table 2). Maximum warming was observed near the continental shelf break, a region directly influenced by the Kuroshio and its intrusive flows^{6,58}, and thereby its heat advection (Fig. 1a,b). Here, SST trends are strongest in winter^{5,6,42,59} owing to a weakening of the East Asian winter monsoon, a corresponding reduction in atmospheric latent heat release^{48,49} and enhancement of warm-water intrusion from the Kuroshio^{4–6,26}.

Warming of the SCS has been slower but more persistent than that of the ECS. SST trends are estimated at $0.14 \pm 0.02\text{ }^{\circ}\text{C dec}^{-1}$ from 1950 to 2021 and $0.14 \pm 0.06\text{ }^{\circ}\text{C dec}^{-1}$ from 1982 to 2021 (Fig. 1e; Supplementary Table 2). These trends are spatially inhomogeneous; enhanced warming rates are evident in the Luzon Strait (between the islands of Luzon and Taiwan) and the northeastern basin (Fig. 1a,b). By contrast, warming in the Bohai–Yellow Seas (BYS) is slightly weaker. Here, average SST trends reached $0.09 \pm 0.07\text{ }^{\circ}\text{C dec}^{-1}$ from 1950 to 2021 and $0.13 \pm 0.10\text{ }^{\circ}\text{C dec}^{-1}$ from 1982 to 2021 (Fig. 1f). However, owing to sparse data sampling and remote-sensing errors arising from land influence, most datasets cannot accurately resolve SST changes in the BYS, and so consensus is lacking on the magnitude and statistical significance of any trends^{5,60}.

Consensus on subsurface trends is also difficult to achieve, owing to a shortage of observations. However, some evidence is available to explain any changes at depths. In the YS, for example, the core temperature of the southwestern portion of the Yellow Sea Cold Mass (YSCM; a subsurface cold-water region, $<10\text{ }^{\circ}\text{C}$, occupying the bottom layer of the central YS in summer) increased by $0.02\text{ }^{\circ}\text{C dec}^{-1}$ from 1958 to 2011 (ref. 56). This warming is linked to warm-water intrusion by the Yellow Sea Warm Current⁶¹, which branches from the Kuroshio, consistent with winter surface warming trends^{56,61}. In contrast, the temperature of the southeastern portion of the YSCM decreased^{57,61,62}. Subsurface warming and salinity increases were also reported more broadly in the ECS and YS, albeit at rates lower than at the surface^{53,59}, indicating enhanced stratification^{10,57}.

Thus, the SAC have undergone pervasive increases in SST, exhibiting warming rates that are subject to regional and seasonal differences. The weakening of the East Asian winter monsoon and heat transport by the Kuroshio are critical in shaping the SST warming patterns, giving rise to a warming hotspot in the offshore ECS and stronger warming rates in winter than in other seasons.

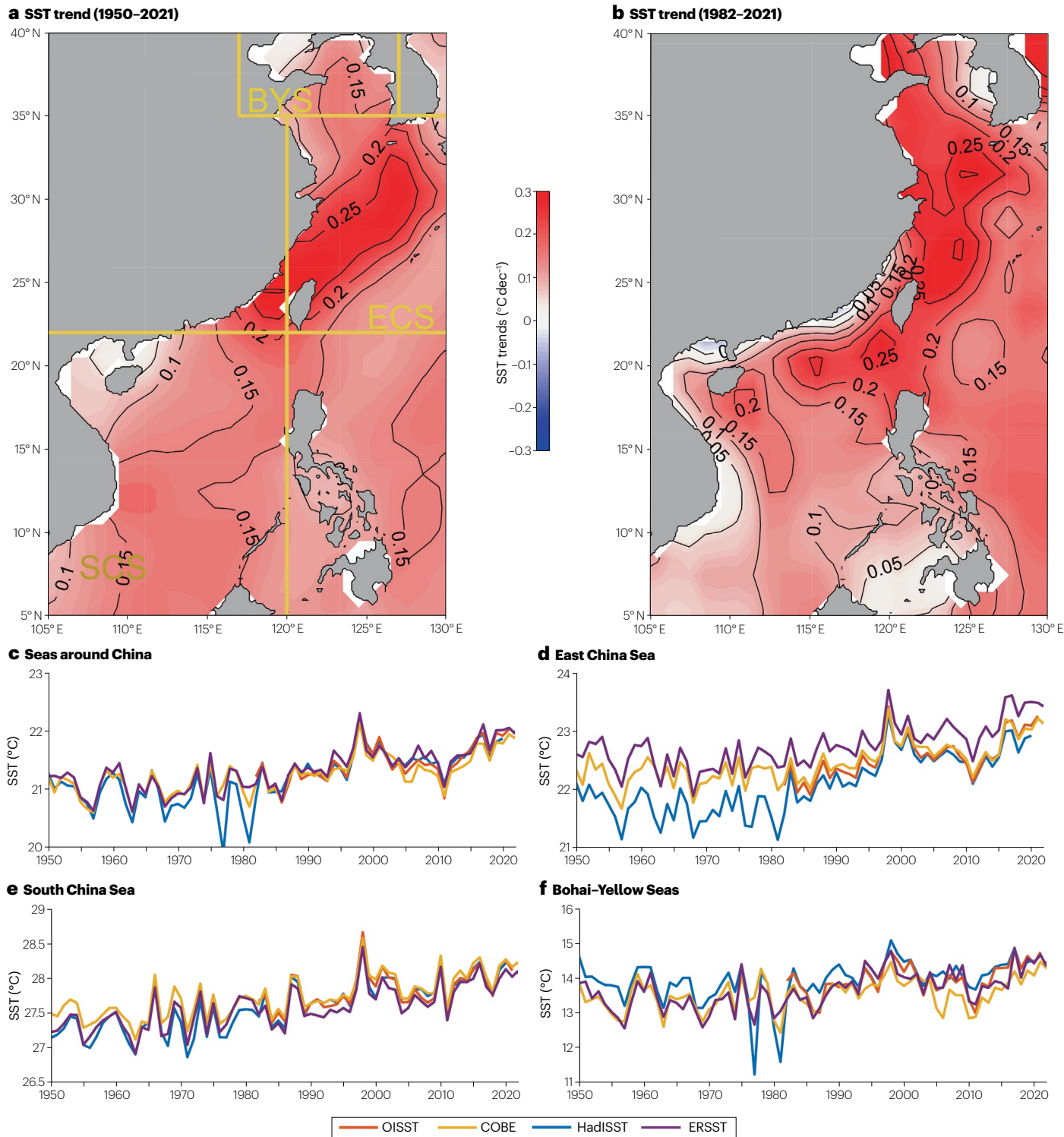


Fig. 1 | Sea surface temperature increases in the seas around China.
a, Sea surface temperature¹⁴ (SST) trends in the seas around China (SAC) during 1950–2021. The yellow lines delineate the East China Sea (ECS), the South China Sea (SCS) and the Bohai–Yellow Seas (BYS). **b**, SST²³⁴ trends during 1982–2021. **c–f**, Annual average SST from various products^{3,44,234,235} for the SAC

(c), ECS (d), SCS (e) and BYS (f). Surface warming has been prevailingly observed across the SAC. COBE, Centennial in situ Observation-Based Estimates; ERSST, Extended Reconstructed Sea Surface Temperature dataset; HadISST, Hadley Centre Sea Ice and Sea Surface Temperature; OISST, Optimum Interpolation Sea Surface Temperature.

Marine heatwaves

Warming trends also increase the likelihood of extreme high temperatures or marine heatwaves (MHWs; typically defined as events lasting more than five consecutive days wherein daily SSTs exceed the 90th percentile of the climatology⁶³) in the SAC^{42,64,65}. Most regions of the SAC experienced over 23 MHW days per year between 1982 and 2014, primarily in summer, with the largest intensities in the BYS²⁸ (Fig. 2).

The frequency and intensity of these MHWs have increased over 1982–2018: annual MHW days increased by 20–30 days dec⁻¹, duration by 5–9 days dec⁻¹, frequency by 1–2 dec⁻¹, and intensity by 0.1–0.3 °C dec⁻¹ (ref. 29). Indeed, during 2016–2018, unprecedented MHWs occurred in the ECS and YS, with a maximum intensity of 3 °C and a maximum duration of 44 days; these events were primarily attributed to increased surface solar radiation and ocean heat advection driven by monsoon variability^{26,65,67}. Conversely, summertime MHWs in the SCS were associated with the intensified northwest Pacific subtropical high, which suppressed the summertime wind-driven upwelling^{27,66}. MHWs in the northern SCS were driven by both anomalous surface heat fluxes and ocean current advection^{68,69}.

Circulation

Changes in the ocean circulation of the SAC have strong bearing on temperature responses, especially those pertaining to the Kuroshio (Supplementary Fig. 1). These observed changes to the Kuroshio vary regionally along its path, but are often highly uncertain owing to short records, natural variability, inadequate understanding of circulation features and dynamics, and difficulties in modelling. Nevertheless, key changes in circulation features can be determined.

The ‘nascent’ Kuroshio – the Kuroshio at its origin east of Luzon^{70,71} – has been strengthening since the 1990s (ref. 72). This strengthening is related to an intensification of the northeasterly trade winds in the tropical Pacific^{72–78}, a subsequent increase in the transport of the North Equatorial Current^{73,79}, and a southward migration of its bifurcation point off the Philippine coast^{72,74–77} which allows more water of the North Equatorial Current to join the Kuroshio. As a result, intrusion of the Kuroshio into the SCS through the Luzon Strait decreased by -0.24 Sv yr^{-1} during 1993–2010 (refs. 76,77,80).

This reduction has been linked to the enhanced inertia of the Kuroshio along with the weakened monsoon. Physically, the weakened monsoon reduces the zonal pressure gradient and Ekman transport that maintain the westward transport through the Luzon Strait⁷⁶; meanwhile, the enhanced nascent Kuroshio tends to leap across the strait owing to its high inertia rather than penetrating into the SCS as a loop current⁸¹. By contrast, the deep-water transport into the SCS across the Luzon Strait increased by -9% during 2009–2021 (ref. 82). Full-depth overflow estimates in the Luzon Strait suggest an overall reduction of $-0.43 \text{ Sv dec}^{-1}$ during 2003–2016 (ref. 83).

The surface intensity of the Kuroshio east of Taiwan also increased from the 1950s to the 2000s⁸⁴. At the Pollution Nagasaki section (from 30 °N, 124.5 °E to 27.5 °N, 128.25 °E), the Kuroshio volume transport increased by -0.47 Sv during 1955–2010 (ref. 9). However, prominent decadal variations are embedded within this longer-term increase^{84–87}: the Kuroshio east of Taiwan decreased by -0.7 Sv dec^{-1} from 1992 to 2013 owing to weakened North Pacific wind stresscurls and impinging mesoscale eddies⁸⁵; and the Kuroshio at the Tokara Strait decreased by -0.5 Sv dec^{-1} during 1998–2013 owing to basin-scale wind anomalies associated with the negative PDO phase⁸⁷.

Changes to the monsoon also drove corresponding impacts to other circulation features in the SAC, including more frequent

cross-shelf intrusions of the Kuroshio water into the ECS^{6,54}; a 10% weakening of the winter cyclonic circulation in the upper SCS from 1959 through 2008 owing to a reduction of the wind stress curl⁸⁸; weakening of the SCS abyssal circulation during 2003–2016 (ref. 89); a strengthening of the Taiwan Strait current from 1993 to 2010 due to amplified meridional sea surface height difference; and an increase in the intensity of the Zhe-Min coastal current during 1999–2016 (refs. 90–92).

Historical biogeochemical changes

Changes in the biogeochemical properties of the SAC have accompanied warming and circulation changes, coupling physical and biological processes. Changes in nutrient content, hypoxia, acidification and carbon storage in the SAC are now discussed.

Nutrients

Cumulative anthropogenic nutrient input through atmospheric deposition and river and groundwater discharges has led to pervasive coastal-water increases⁹³ in dissolved inorganic nitrogen (DIN), dissolved inorganic phosphorus (DIP), and the relative abundance of nitrogen to phosphorus, N^* ($N^* = \text{DIN} - R_{\text{Redfield}} \times \text{DIP}$, where $R_{\text{Redfield}} = 16$, the Redfield ratio)⁹⁴.

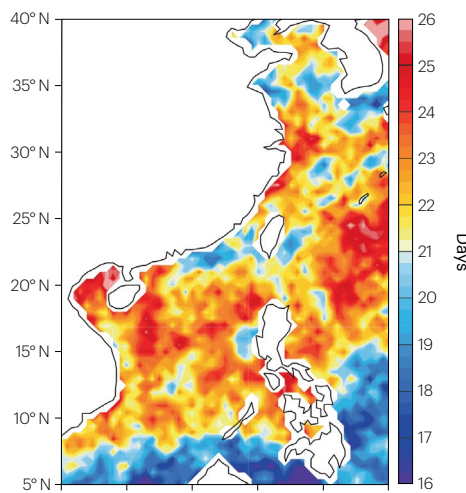
Indeed, DIN has increased across all subregions of the SAC, albeit with substantial temporal variability, owing to atmospheric deposition^{95–100}, riverine discharge such as from the Yangtze and Pearl Rivers^{101,102}, and input from ocean currents such as the Kuroshio^{103–105}. In the BYS, for example, DIN concentrations increased 7-fold, from $<3 \mu\text{mol l}^{-1}$ in the late 1950s to $>22 \mu\text{mol l}^{-1}$ in the mid-2010s (refs. 97,106–109). Similarly, DIN concentrations in the ECS exhibited a persistent upward trend, from $<4 \mu\text{mol l}^{-1}$ in the early 1980s to $>11 \mu\text{mol l}^{-1}$ in the mid-2010s, and an acceleration since 2007, coincident with changes at the Yangtze River estuary (YRE) since the 1980s. However, DIN changes in the eastern ECS are not as clearly apparent, owing to a lesser influence of Yangtze River discharge and a stronger influence of the Kuroshio^{97,104}. In the northern SCS, DIN increased from $1.7 \mu\text{mol l}^{-1}$ in 1989 to $10.8 \mu\text{mol l}^{-1}$ in 2001 (ref. 109), as also evidenced from historical observations in the Pearl River estuary (PRE) over 1986–2017 (Supplementary Fig. 2; ref. 102).

As a result, N^* and the nitrogen-to-phosphorus ratio (N/P) have also increased across most of the SAC, with the rising DIN dominating these responses. N^* strongly increased in the BYS during the 1990s and 2000s, with rates of 0.33 , 0.26 and $0.21 \mu\text{mol kg}^{-1} \text{yr}^{-1}$ in the BS, northern YS and southern YS, respectively⁹⁶. In the ECS, N^* exhibited a longer-term increase since 1980, broadly reflective of changes in the northern SCS and the PRE^{102,109}. In most cases, these changes in N^* reflect a transition in phytoplankton from nitrogen-limited systems to phosphorus-limited systems during the 1990s or 2000s^{93,100,110}.

Hypoxia

Hypoxia describes waters with dissolved oxygen concentrations below certain criteria, such as 63 or $94 \mu\text{mol l}^{-1}$. An increasing number of offshore hypoxic waters have been observed since the 1960s. Their occurrence is driven by two primary preconditions (Fig. 3a,b): stratification, which hinders the supply of oxygen from the sea surface to the bottom water, especially below the thermocline^{111,112}; and a rich supply of surface nutrients that fuels primary production, increasing organic matter transport to the bottom water, the degradation of which consumes dissolved oxygen^{111,112}. Nutrient transport from rivers or the Kuroshio intrusion often fulfills this second criterion^{113–115}. Topography¹¹⁶, tides¹¹⁷, bottom sediment respiration¹¹⁵, monsoon and typhoon winds¹¹⁸, and groundwater discharge¹¹⁹ are additional influencing factors.

a Observed MHW days (1982–2014)



b Observed MHW intensity (1982–2014)

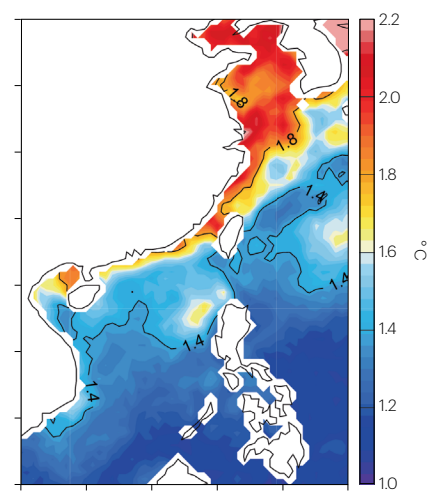
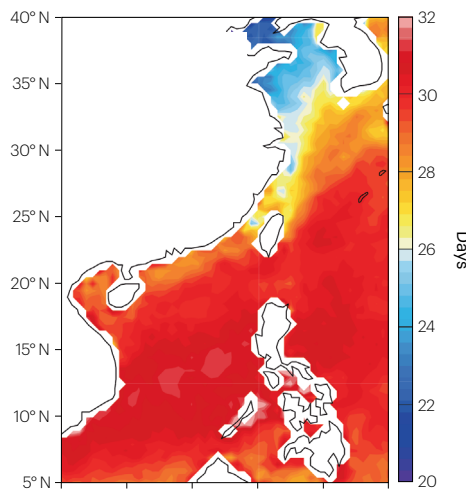


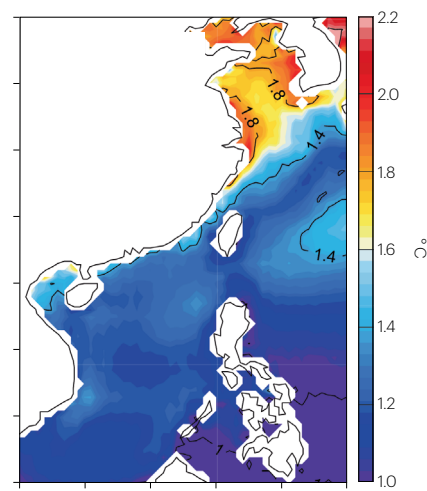
Fig. 2 | Observed and projected marine heatwaves in the seas around China. **a,b**, Observed²³⁴ marine heatwave (MHW) days per year, and average MHW intensity (maximum SST anomaly over the duration of the MHW) during 1982–2014, respectively.

c,d, As in **a** and **b**, but the multimodel mean MHW days and intensity from 24 CMIP6 models²⁰⁰ with historical forcing. **e,f**, As in **c** and **d**, but multimodel mean MHW days and intensity over 2051–2080 from CMIP6 models forced with a moderate emission scenario (Shared Socioeconomic Pathway 2-4.5). MHWs are becoming more frequent and stronger across the seas around China.

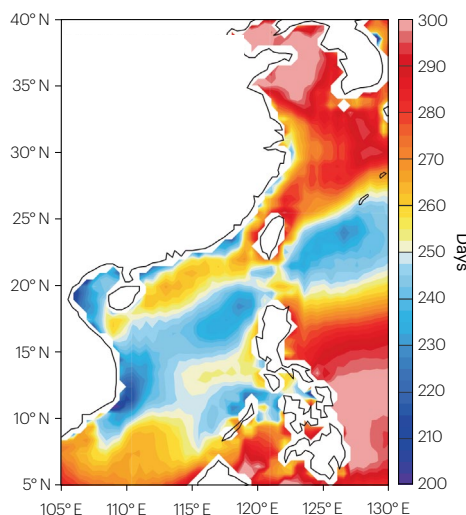
c Simulated MHW days (1982–2014)



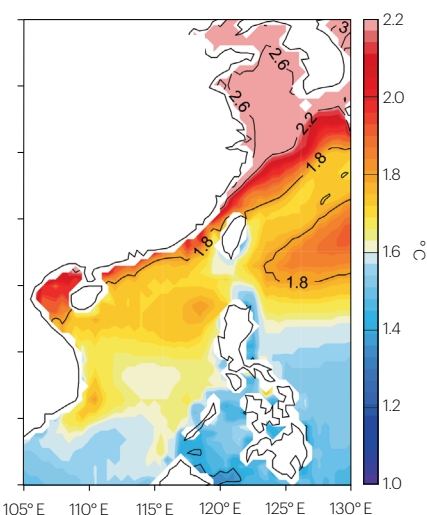
d Simulated MHW intensity (1982–2014)



e Projected MHW days (2051–2080)



f Projected MHW intensity (2051–2080)



a Biogeochemical processes in normal conditions

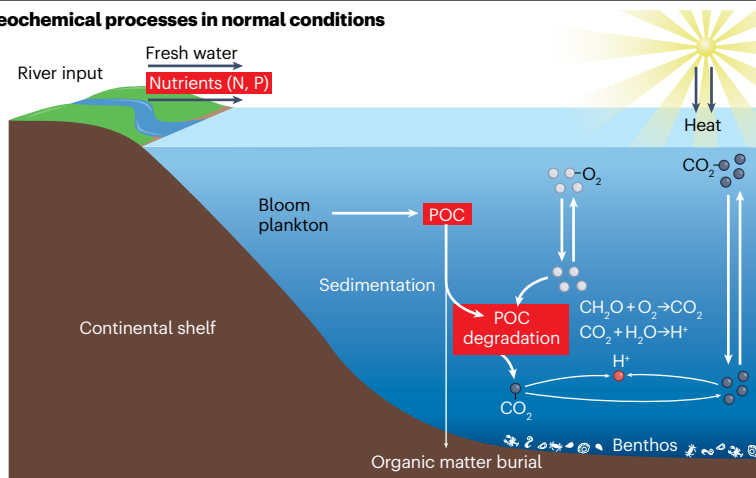
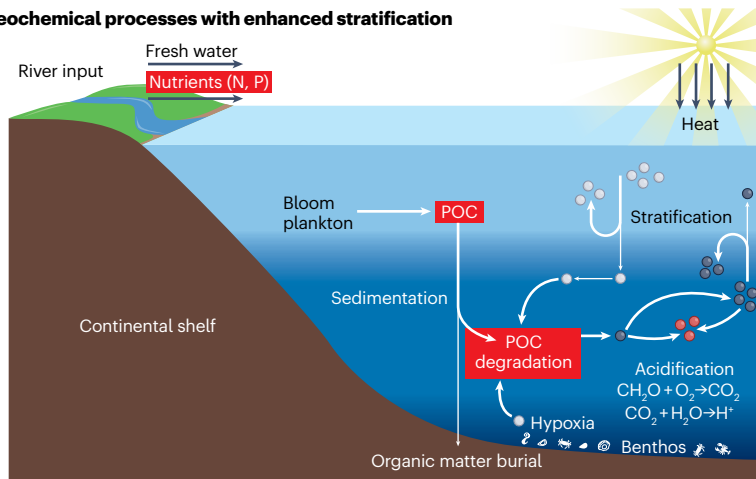
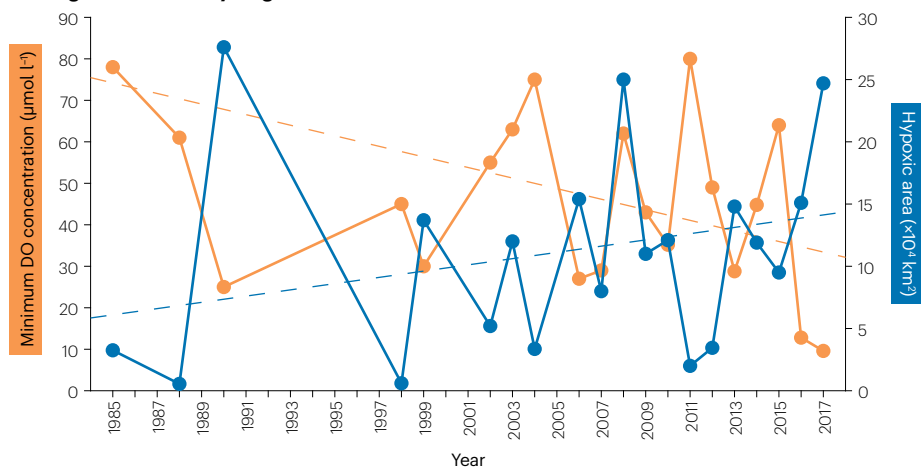


Fig. 3 | Observed changes in hypoxia and acidification. **a,b**, Schematic descriptions of biogeochemical processes under normal (**a**) and enhanced (**b**) stratification conditions. POC, particulate organic carbon. **c**, Historical changes in the hypoxic area (blue) and minimum dissolved oxygen (DO) concentration (yellow) in the Yangtze River estuary^{236–242}. The dashed lines indicate linear fitting for the trend. Enhanced stratification owing to surface warming leads to hypoxia and acidification, as seen in the Yangtze River estuary.

b Biogeochemical processes with enhanced stratification



c Yangtze River estuary biogeochemical conditions



Although permanent hypoxia has not yet been observed in the SAC, seasonal hypoxia of bottom waters has been ubiquitously observed^{11–13,120–123}, albeit with substantial temporal and event-based variability¹²⁴. For example, bottom-water hypoxia in the Mirs Bay and

northern SCS occurs mainly during July–September¹³, whereas in the YRE, it develops in late spring or early summer, peaks in August, decays in autumn and demises in winter¹²⁵; hypoxia in the PRE occurs sporadically in time and location, without a regular seasonality¹²¹.

Despite pronounced interannual variability, a long-term deoxygenation trend is robust in the YRE, as suggested by the increasing hypoxic area and decreasing minimum dissolved oxygen concentration (Fig. 3c). Specifically, the minimum dissolved oxygen concentration and the hypoxic area changed from $78 \mu\text{mol l}^{-1}$ and $3.3 \times 10^4 \text{ km}^2$ in 1985 to $9.6 \mu\text{mol l}^{-1}$ and $24.7 \times 10^4 \text{ km}^2$ in 2017, respectively. More broadly, in situ observations and inversion results based on redox-sensitive elements (molybdenum, vanadium and uranium) in sediments suggest that the severity of hypoxia in the SAC is increasing^{123,126,127}. For example, the bottom-water dissolved oxygen in the PRE showed a decreasing trend of $2.0 \pm 0.9 \mu\text{mol kg}^{-1} \text{ yr}^{-1}$ over the past 25 years¹²³; sediment records also suggest a decline of bottom-water dissolved oxygen since the mid-1980s in the YRE^{126,127}. These changes are consistent with increasing SSTs that enhance stratification favouring hypoxia and have implications for N_2O release (as in the YRE¹²⁸), organic matter preservation in sediments¹²⁹, and release of elements such as arsenic and phosphorus³⁰.

Acidification

Enhanced stratification arising from rising SSTs also has bearing on coastal-water acidification. Stratification, along with river discharge, degrades eutrophication-related particulate organic carbon in the bottom water, consuming dissolved oxygen and releasing CO_2 , which accumulates to reduce the pH in bottom waters^{116,130} (Fig. 3a,b). Thus, low pH regions in the SAC typically coincide with hypoxic waters, as seen in the YRE and the YSCM^{116,131}. However, this overlap is not always synchronous, as demonstrated by Mirs Bay bottom-water pH being lowest in July, but dissolved oxygen concentrations being lowest in August¹³.

As with hypoxia, longer-term changes in pH have been observed across the SAC. Indeed, repeat surveys reveal a decreasing summertime bottom-water pH at an average rate of 0.019 dec^{-1} in the BS during 1978–2013 (ref. 132). Similarly, winter bottom pH in the northern YS has decreased by $0.011 \pm 0.009 \text{ dec}^{-1}$ over 1976–2016 (ref. 122). Continuous observations in the coastal waters of the ECS also reveal emerging acidification from 2002 to 2011 (ref. 133). Although these changes can be partly attributed to warming and corresponding changes in stratification, the discharge of low pH sewage, the high concentration of dissolved inorganic carbon, surface carbon uptake and nutrient distribution also contribute to acidification^{134–136}.

Carbon storage

The SAC are an important component of the regional carbon cycle. Broadly, they represent a net carbon sink, contributed by carbon fixation flux ($854.76 \text{ TgC yr}^{-1}$; $1 \text{ Tg} = 10^{12} \text{ g}$), riverine inputs ($112.99–115.79 \text{ TgC yr}^{-1}$), oceanic inputs ($64.72–121.17 \text{ TgC yr}^{-1}$), the biological pump (depositional export to sediments; $20.49 \text{ TgC yr}^{-1}$) and the microbial carbon pump (the conversion and output of recalcitrant dissolved organic carbon) (ref. 15). Coastal wetlands, including mangroves, salt marshes and seagrass bed ecosystems, also account for a carbon uptake of 0.97 TgC yr^{-1} (ref. 17), complemented by $>1.0 \text{ TgC yr}^{-1}$ by mariculture¹¹¹.

In the context of air-sea exchange, the SAC probably serve as a source of atmospheric CO_2 , with a net release of $6.01–9.33 \text{ TgC yr}^{-1}$ (ref. 15) or $9.5 \pm 53.0 \text{ TgC yr}^{-1}$ (ref. 137). However, these estimates are highly uncertain, owing to limited data sampling and temporal variability. For example, observations of surface-water $p\text{CO}_2$ (partial pressure of CO_2) in the SCS during 2000–2018 suggest a flux estimate of $13.3 \pm 18.8 \text{ TgC yr}^{-1}$ (ref. 138), much lower than the earlier estimate of $33.6 \pm 51.3 \text{ TgC yr}^{-1}$ (refs. 137,139). This difference is large enough to reverse the sign of the total flux CO_2 from the SAC¹⁴⁰ from a source of $9.5 \pm 53 \text{ TgC yr}^{-1}$ to a sink of $-10.8 \pm 23.1 \text{ TgC yr}^{-1}$.

The effect of a warming climate on the carbon flux of the SAC is difficult to infer. Generally, continental shelf carbon sinks are predicted to decline^{141,142}, owing to the reduced solubility of CO_2 in warmed seawater¹⁴³ and modified primary production and community assemblages¹⁴⁴. However, observations suggest that the global uptake of CO_2 by marginal seas was overall increasing since the 1990s¹⁴⁵. In the SCS, for example, this increase is supported by a positive trend of surface $p\text{CO}_2$ of $2.5 \pm 1.0 \mu\text{atm yr}^{-1}$ since 2000 (ref. 145).

Historical biological changes

The physical and biogeochemical changes observed in the SAC, in turn, influence primary productivity, species distribution range, and biodiversity across plankton (Fig. 4), benthos, and fish communities, as now discussed.

Plankton

Primary productivity. Chlorophyll- α (Chl- α) reflects the biomass of marine phytoplankton and is used as a broad measure of marine productivity¹⁴⁶. Satellite estimates, such as from the Moderate Resolution Imaging Spectrometer (MODIS)¹⁴⁷, reveal complex spatiotemporal changes in surface Chl- α concentration across the SAC^{18,20,93,148,149} owing to often-competing drivers. Although increases in the terrestrial nutrient input promote the growth of phytoplankton in coastal waters^{18,20,111,148,149}, SST warming can either enhance primary productivity (by intensifying coastal winds in upwelling regions and entraining nutrient-rich subsurface water into the euphotic zone^{150,151}) or reduce primary productivity (by enhancing near-surface stratification and hindering upward nutrient supply⁹³).

Generally, Chl- α concentrations increased up until the early-mid 2000s, with the specific timing dependent on the region examined. In the BS, for example, Chl- α concentrations increased 2–3-fold from the early 1980s to the early 2010s (refs. 20,111,148). In contrast, the southern YS exhibited an overall increase from 0.2 to 0.8 mg m^{-3} from the 1990s to 2008 (ref. 149), and in the ECS, Chl- α concentrations increased from 0.95 to 1.28 mg m^{-3} during 1979–2014 (ref. 18). A similar increase was also observed in the northern SCS during 1997–2003, rising by 12%^{19,152}. These increases can broadly be linked to eutrophication induced by industrial and domestic nutrient discharge through rivers, changes in monsoonal winds, and ocean warming, with the contributions of the various drivers differing depending on the region.

After this increase, however, Chl- α concentrations tend to decline. For instance, the concentration of surface Chl- α rapidly decreased by 20% after ~2012 in the BYS (Supplementary Fig. 3). The increase also reversed in the YS and ECS from the early 2000s. Indeed, in situ measurements in Jiaozhou Bay (off Shandong coast in the western YS), a representative region for the coastal-water plankton of the YS, decreased from 3 mg m^{-3} to 1 mg m^{-3} from 2001 to 2015 (Fig. 4b); total phytoplankton showed a consistent reduction (Fig. 4c). Offshore regions of the YS and ECS indicate a similar decline since the 2000s, linked to enhanced seawater stratification owing to SST warming¹⁵³. More broadly, these changes can be linked to the phase shift of the PDO, whereby warm SST anomalies reduce rainfall, suppressing terrestrial nutrient input¹⁵⁴. Seasonality and interannual variability driven by monsoonal winds, the Kuroshio intrusion and ENSO are also considerable^{152,155,156}.

Phytoplankton. In addition to changes in plankton abundance, there have been shifts in phytoplankton species composition, primarily owing to warming SSTs. Generally, the number and abundance of warm-water phytoplankton species have increased in the SAC. In Jiaozhou Bay,

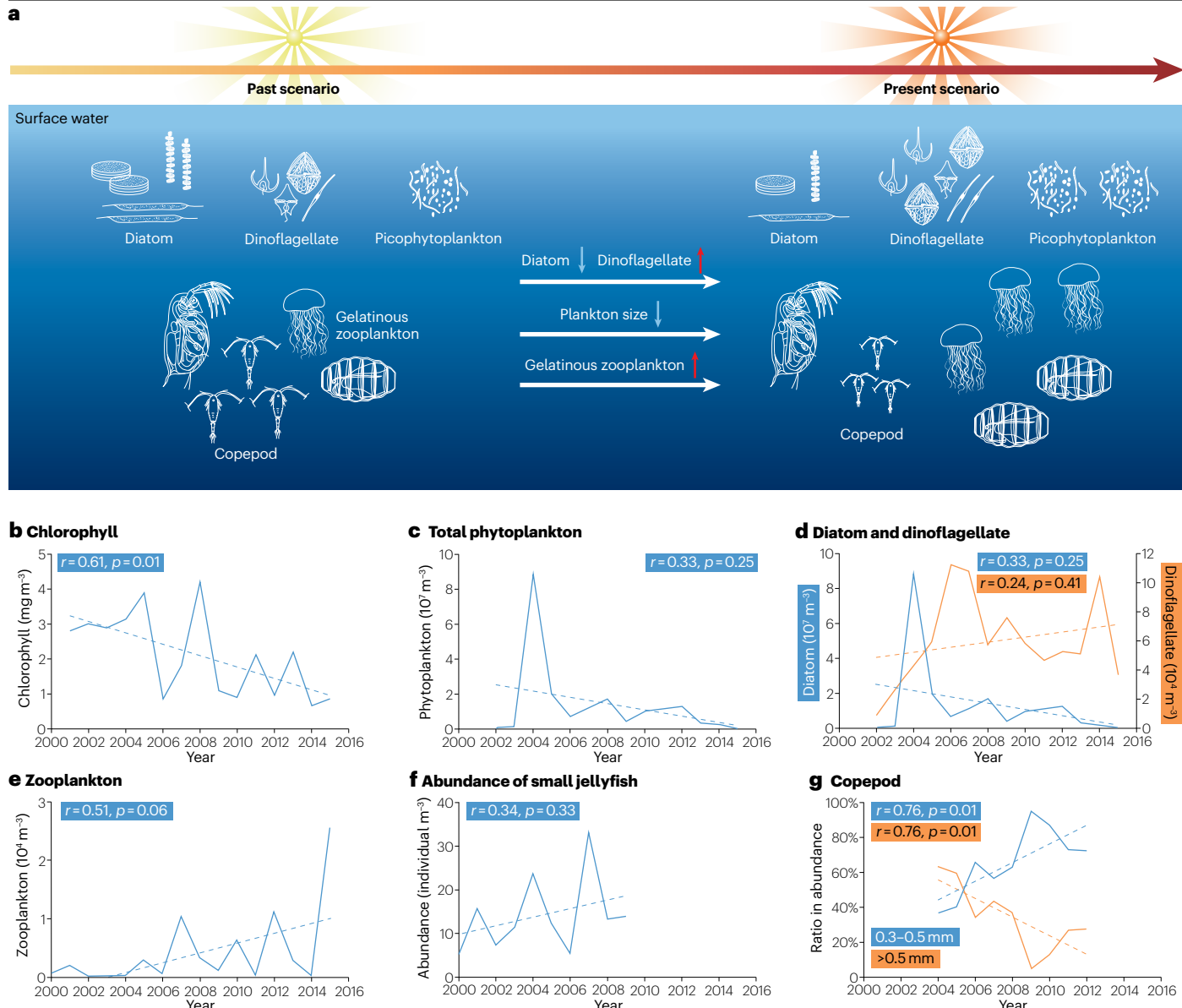


Fig. 4 | Changes in plankton communities. **a**, A schematic comparison of the plankton communities in the past and the warmer present. **b–g**, Changes in plankton communities in Jiaozhou Bay, broadly representative of the Yellow Sea, based on available observational data^{166,243,244}: surface chlorophyll- α concentration (**b**), total phytoplankton cell abundance (**c**), cell abundances of diatoms (blue) and dinoflagellates (yellow) (**d**), zooplankton abundance (**e**), total abundance of small jellyfish (**f**), collectively including all jellyfish species with a

typical size of 1 cm or less), and the abundance ratios of small-sized (0.3–0.5 mm; blue) and large-sized (>0.5 mm; orange) copepods (**g**). Dashed lines indicate linear fits with the respective correlation coefficients r and the p values. With warming, major changes include an increase in the ratio of dinoflagellate to diatom cell abundance, a decrease in plankton size and an increase of gelatinous zooplankton (small jellyfish).

for instance, warm-water species increased since the 1980s (ref. 156). Similarly, in the Taiwan Strait, the proportion of phytoplankton classed as warm-water phytoplankton species was 7.3% higher in 2006–2008 than in 1984–1985 (ref. 157). The dominant phytoplankton species in the YRE also shifted from temperate–subtropical to subtropical–tropical taxa from 1995 to 2009 (ref. 158).

Alterations in the phytoplankton community structure have further been detected, with the increasing dominance of dinoflagellates as

a prevailing feature. These changes can be linked to an increase in N/P ratio (Supplementary Fig. 2), a transition from nitrogen to phosphorus limitation, and a resulting increase in dinoflagellates (at the expense of diatoms) who can use dissolved organic phosphate^{110,153,158–160}. In the BS, the present-day ratio of dinoflagellate to diatom cell abundance is 2.82 times as high as that in the twentieth century, representing a shift from a diatom-dominated community to one co-dominated by diatom and dinoflagellate species¹⁶¹. Similar shifts have been observed in the YS,

where the ratio of dinoflagellate to diatom cell abundance was twice as high in 2005–2015 as in 1985–2000 (ref. 21), and the dominance of *Ceratium* and *Noctiluca* in dinoflagellate species also increased¹⁵³. The Jiaozhou Bay witnessed decreasing diatoms and increasing dinoflagellates during 2002–2016 (Fig. 4d).

Another observed trend in the phytoplankton community structure is miniaturization (Fig. 4a). Enhanced water stratification and nutrient-depleted conditions in surface waters favour small-sized phytoplankton cells; their high surface area to volume ratio enables more efficient nutrient exchange with surrounding water¹⁶². In Jiaozhou Bay, for example, the proportions of micro-phytoplankton and nano-phytoplankton have decreased and increased, respectively¹⁶³. Similar changes have also been observed in the Taiwan Strait¹⁵⁷ and in the SCS, with the proportion of phytoplankton in the pico-size class (<2 µm) increasing substantially in the latter region over 2003–2018 (ref. 164).

Zooplankton. Changes have also been apparent in zooplankton abundance. The abundance of gelatinous zooplankton has concurrently increased in the SAC, except for the SCS¹⁶⁵. For example, the abundance of small jellyfish in Jiaozhou Bay was five times as large in the 2000s as in the twentieth century¹⁶⁶ (Fig. 4e,f). The frequency of small and giant jellyfish outbreaks (*Doliolum* and *Nemopilema nomurai*, specifically) also increased substantially since ~2000 in the YS and ECS^{167–169}. Increasing abundances of *Oikopleura dioica* and *Eirene ceylonensis*, as well as jellyfish blooms, have also been observed in the BS¹⁷⁰.

Like phytoplankton, changes in zooplankton community structure have been observed. The distribution range of warm-water zooplankton species showed a northward expansion in response to ocean warming. Specifically, the dominance of warm-water species, such as *Centropages tenuiremis*, *Centropages dorsispinus*, *Clytia hemisphaerica* and *Pleurobrachia globosa*, increased in the Bohai Bay from 2004 to 2015 (ref. 171). Moreover, *Sagitta enflata* and *Doliolum denticulatum*, which were not observed in 1959, were observed in the northern YS in 2009 (ref. 22). Additionally, the abundance of *Euphausia pacifica* (a cold-water zooplankton species) decreased substantially in the ECS, as it migrated in response to warming²³.

Furthermore, zooplankton miniaturization has been detected in several regions; ocean warming selectively favours smaller organisms¹⁷² because they often exhibit higher fecundity and growth rates when there is adequate food supply in warmer waters¹⁷³. As a result, the abundance of large copepods, such as *Calanus sinicus* and *Labidocera euchaeta*, decreased, whereas that of small copepods, such as *Acartia pacifica* and *Centropages dorsispinus*, increased in the BS during 2004–2015 (ref. 171). These features are echoed in Jiaozhou Bay, where the proportion of small-sized copepods increased, and the mean size of all copepods decreased¹⁶⁷ (Fig. 4g).

Benthos

Changes in plankton communities, along with direct impacts of physical (such as from MHWs¹⁷⁴) and biogeochemical changes (such as from hypoxia and acidification^{175–177}), could have important ramifications for trophic interactions through bottom-up control, altering community structures of higher-level organisms such as benthos (bottom-dwelling organisms)¹⁷⁸.

Despite the sparsity of observational records in most parts of the SAC, changes in benthic ecosystems have been identified. In the YS, for example, there has been an overall reduction in benthic diversity^{34,35,179,180}. A corresponding change in community structure has also been observed, including an 81.4% increase in abundance of small

mollusks¹⁸⁰ and a 55.7% increase in the biomass of small polychaetes³⁴ since the 1980s. The distribution of some intertidal benthos has further shifted northward by ~3 degrees in latitude^{181,182} during the past several decades. Owing to acidification, clams, scallops, mussels and oysters have exhibited increased sensitivity, increased likelihood of mortality, reduced clearance rate (97%), disturbed biomineralization and protein expression patterns, and decreased growth rate (6–16% smaller in length) and survival rate (by 40%) during the larval stage^{183–186}.

The co-occurring impacts of hypoxia and acidification on marine benthos have also been observed in the BS, YRE, PRE and some areas of the SCS^{120,187}. For example, bottom-water hypoxia and acidification are responsible for the failure of scallop breeding¹⁸⁷. The warming, acidification and eutrophication in the northern YS have caused increasing stress on marine calcifying organisms and benthic ecosystems¹²⁰.

However, the influences of a warming climate on benthic ecosystems are heavily entwined with other anthropogenic effects. For example, in Jiaozhou Bay, the abundance and biomass of macrobenthos decreased by ~50% throughout the 1980s (Supplementary Table 4) owing to the effects of pollution, construction, aquaculture and overfishing¹⁷. The abundance and biomass of the macrobenthos have recovered since the 2000s, demonstrating the importance of considering the combined influences of physical, biogeochemical, and anthropogenic factors when discerning ecological changes.

Fish and fishery resources

Marine fish are sensitive to water temperature changes¹⁸⁸. Therefore, ocean warming has altered the phenology¹⁸⁹, body size¹⁹⁰, distribution range^{191,192} and productivity^{191,193} of marine fish in many regions across the globe, including the SAC.

Changes in the distributional range of fish species are particularly evident. Typically, the proportion of warm-water species in fish communities has been increasing^{36,37}, with the mean temperature of catches increasing by 2.46 °C and 1.32 °C during 1950–2010 in the BYS and ECS, respectively (Fig. 5a). Moreover, 13 species of previously unobserved warm-water fish have appeared in the Taiwan Strait since 2000 (ref. 194). A tropical warm-water fish was also observed in the Beibu Gulf of the SCS in 2020 (ref. 14); however, after an initial decrease in the abundance of subtropical species caused by increasing temperatures, the scope for further tropicalization in the SCS is limited, and the overall species richness is projected to decrease by 6–7 under different scenarios^{37,195}.

These changes will consequently influence fishery resources, with China projected to be one of the countries with the highest loss in potential catch and fishery income under a warming climate^{196,197}. Currently, however, total fishery catch in the SAC has increased since 1950 (Fig. 5b), largely reflecting rising catch capability (for example, the number of fishing ships and technological advances) and not the negative impacts of a warming climate¹⁹⁸. Yet it is clear that the large-scale redistribution of fish populations and modified fish communities is likely to have knock-on effects across the SAC, as observed in other regions^{196,199}.

Projected changes

Given the suite of physical, biogeochemical and ecological changes observed across the SAC in the present climate, it can be expected that any such changes might continue, or even be amplified, under the projected warming. These projections are now discussed.

Physical changes

Climate Model Intercomparison Project phase 6 (CMIP6) models²⁰⁰, which broadly reproduce the observed warming pattern (Fig. 6a;

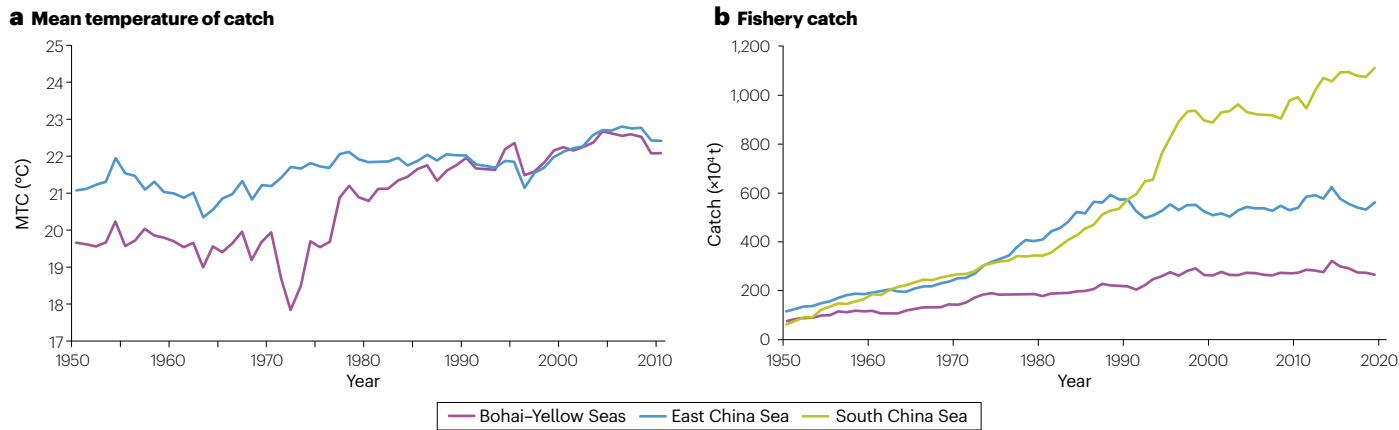


Fig. 5 | Historical changes in fishery catch. a, The mean temperature of catch (MTC) – that is, the average inferred temperature preference of exploited species weighted by their annual catch – in the Bohai–Yellow Seas and the East China Sea.

b, Fishery catches in the Bohai–Yellow Seas, East China Sea and South China Sea³⁷. The seas around China exhibit an increasing proportion of warm-water species in fish communities and increasing total fishery catch.

Supplementary Table 2), provide insights into projected physical changes in the SAC. SST is anticipated to rise across the SAC until at least the 2050s, regardless of the emission scenario considered (Fig. 6b,c). The total change (average SST of 2090–2099 minus that of 2015–2022) is projected to be 3.03 ± 0.78 °C, 1.43 ± 0.54 °C and 0.71 ± 0.52 °C for Shared Socioeconomic Pathways (SSP) 5-8.5, 2-4.5 and 1-2.6, respectively. A persistent warming trend is apparent until the end of the twenty-first century under SSP 5-8.5, compared with thermal equilibrium by ~2060 for the other two scenarios (Fig. 6c). These projections are broadly consistent with those of CMIP5 models, which indicate SAC-wide warming rates of -3.0 and -1.5 °C under the Representative Concentration Pathway (RCP) 8.5 and RCP4.5 scenarios, respectively^{201,202}.

Unlike the observed warming, which was strongest in the ECS (Fig. 1), projected warming is strongest in coastal waters²⁰², especially those of the BYS (Fig. 6c–f). In the ECS, for example, total warming (2090–2099 minus 2015–2022) reaches 3.13 ± 0.64 °C and 1.48 ± 0.41 °C for SSP 5-8.5 and SSP 2-4.5, respectively (Fig. 6d). Temperature changes for the same scenarios are 2.72 ± 0.56 °C and 1.25 ± 0.32 °C for the SCS (Fig. 6e). In contrast, they reach 4.30 ± 1.05 °C and 2.18 ± 0.69 °C for the BYS (Fig. 6f). Although these changes are most pronounced in regions where models have difficulties in simulating important fronts and coastal currents^{57,201}, it is likely that enhanced warming in the BYS is a robust feature, as suggested by regional downscaling projections²⁰³.

As with general warming, CMIP6 models also capture MHWs reasonably well, but tend to overestimate the number of MHW days in the SCS and the eastern ECS and underestimate the average intensity²⁰⁴ (Fig. 2a–d). These models indicate a substantial increase in the number and intensity of MHWs in the future²⁹ (Fig. 2e,f). Specifically, under SSP 2-4.5 and assuming the present-day climatology, by 2051–2080, MHWs in the BYS and the ECS will exceed 270 days per year and reach 1.8–2.6 °C in average intensity, in contrast to the 20–23 days per year and 1.4–1.9 °C intensity in the historical period (Fig. 2a,b). Adopting the stationary-threshold definition, projections under the SSP 5-8.5 scenario suggest that the global ocean will experience all-year-around MHW conditions by the late twenty-first century^{29,63,204,205}; however, the definition of MHWs, particularly the choice of threshold, is still under debate.

Model simulations also suggest the robust emergence of long-term trends in ocean circulation under anthropogenic climate change^{206–209}.

The major western boundary currents, including the Kuroshio, are likely to strengthen and shift poleward²⁰⁷. CMIP6 models project an acceleration of the global surface circulation and a deceleration of the lower-thermocline circulation in response to SST warming²⁰⁹. Correspondingly, the Kuroshio is projected to accelerate in the upper 500 m but decelerate at greater depths²⁰⁶. Meanwhile, the Kuroshio transport in the ECS is also projected to increase²⁰³. CMIP5 projections under middle and high emission scenarios indicate that the cross-shelf inflow and outflow (crossing the 100-m isobath) in the ECS–YS region will increase by 0.42 and 0.48 Sv from 2006 to 2099, respectively²¹⁰. Despite minimal changes in the net transport, this increase could indicate an enhanced exchange between the Kuroshio and the ECS–YS shelf.

Biogeochemical and biological changes

In comparison with ocean temperatures and circulations, it is more challenging to project biogeochemical and biological changes, owing to the fundamental deficiencies in model dynamics. Thus, there are few regional projections of the biogeochemical and biological changes in the SAC. Some understanding of future changes has, however, been gleaned.

The severity of deoxygenation and acidification is likely to increase. In the ECS, in particular, dissolved oxygen concentration decreases of 10.90 ± 3.92 $\mu\text{mol l}^{-1}$ (6.3%) and pH declines of 0.36 ± 0.02 are anticipated by the end of this century under the RCP8.5 relative to 1980–2005 levels. These changes are broadly in keeping with, or exceed, those of global-based estimates^{140,211}. Global increases in river export of nitrate and phosphate²¹² will also have bearing on biogeochemical changes across the SAC, maintaining or increasing the high N/P ratio of the SAC^{213,214}.

At present, changes in plankton biomass and primary productivity cannot be projected with confidence in the SAC, owing to multiple drivers and their potentially competing effects. Generally, however, marine primary productivity is expected to decline in open oceans as surface warming – and thereby enhanced stratification – continues²¹⁵. Similar trends are anticipated for coastal waters of the SAC²⁰². Observed trends in benthos are also likely to continue in the future^{216,217}, with the area occupied by certain cold-water species shrinking as they are replaced by intruding warm-water species²¹⁸. Offshore fish in the SAC

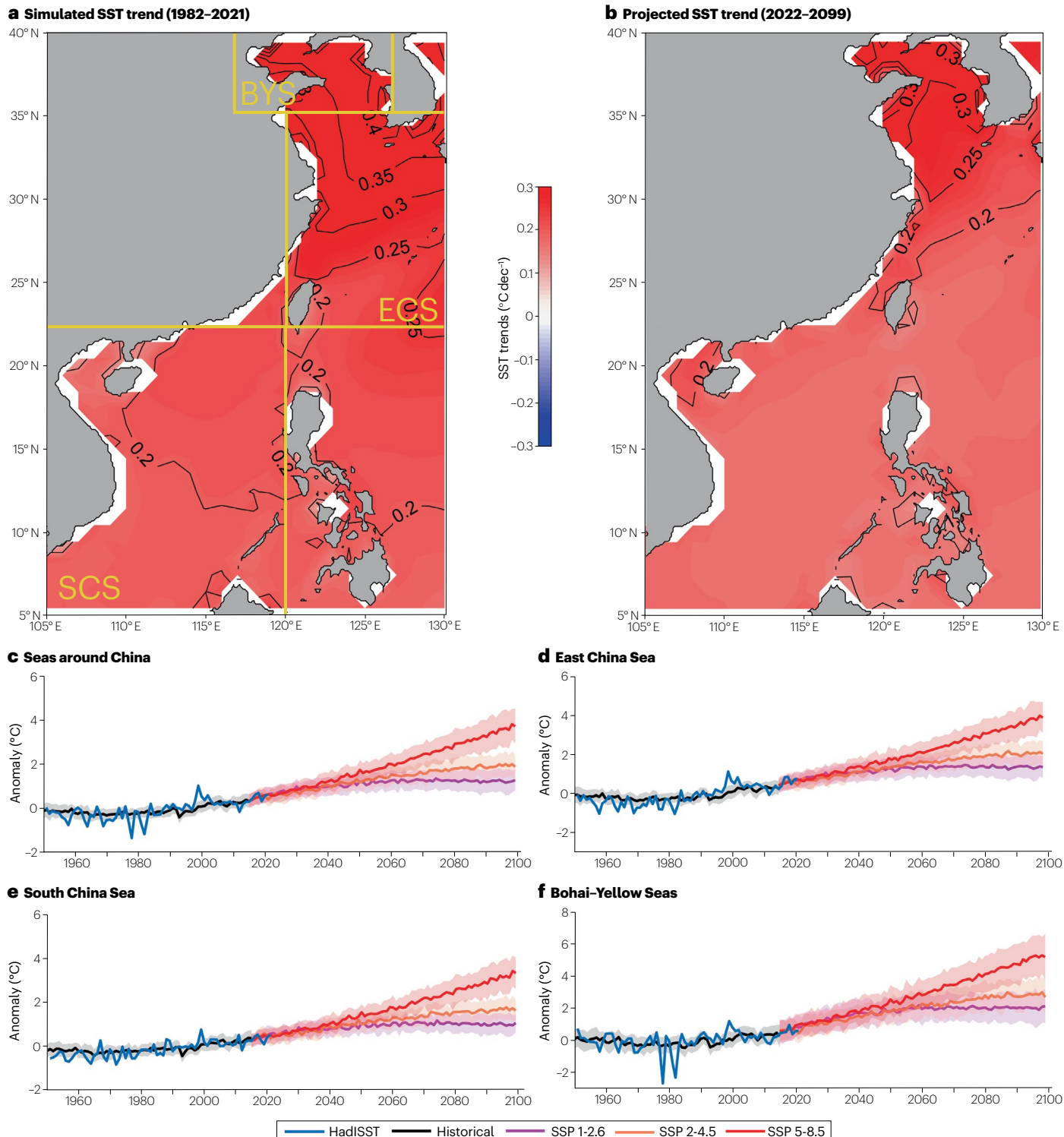


Fig. 6 | Sea surface temperature projections. **a**, Multimodel mean sea surface temperature (SST) trends over 1982–2021 from CMIP6 historical simulations (1982–2014) and the Shared Socioeconomic Pathways (SSP) 2–4.5 projection (2015–2021). **b**, As in **a**, but for 2022–2099 derived from SSP 2–4.5 projections. **c–f**, Regional average SST anomalies for the seas around China (**c**), East China Sea

(**d**), South China Sea (**e**) and the Bohai–Yellow Seas (**f**; note scale), derived from historical simulations (1960–2014) and projections (2015–2099) of SSP 1–2.6, SSP 2–4.5 and SSP 5–8.5. Shading denotes one standard deviation. SST anomalies from Hadley Centre Sea Ice and Sea Surface Temperature (HadISST⁴⁴) are plotted for comparison. SST warming is projected to continue to at least the 2050s.

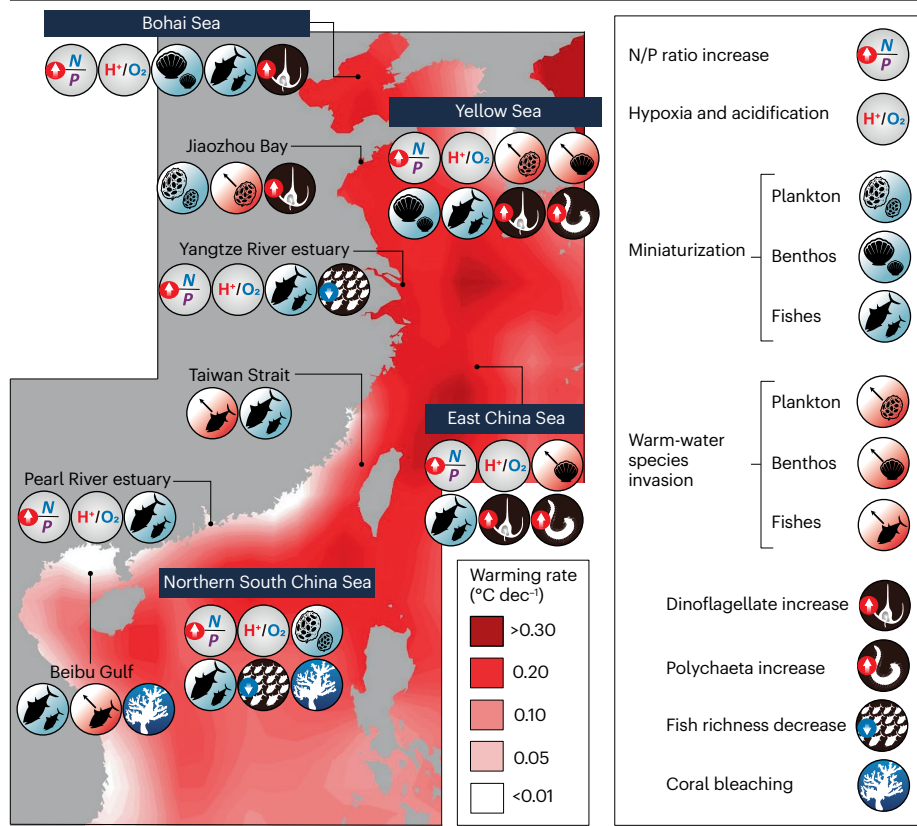


Fig. 7 | Historical changes in the seas around China. The colour shading denotes the observed²³⁴ surface warming rate during 1982–2021. Increased N/P (nitrogen-to-phosphorus concentration ratio), hypoxia and acidification, decreased fish richness and changes in biodiversity are shown for major seas (the Bohai Sea, Yellow Sea, East China Sea and northern South China Sea) and key coastal-water regions (the Jiaozhou Bay, Yangtze River estuary, Taiwan Strait, Pearl River estuary and Beibu Gulf). Major biodiversity trends detected in the seas around China include miniaturization (down-sizing), warm-water species invasion, dinoflagellate increase and polychaeta increase.

are further projected to migrate 110–206.5 km poleward on average under different warming scenarios¹⁹⁵. Changes in the distribution of marine fish will alter the distribution of potential catch and affect fisheries production, but there are multiple challenges involved with projecting changes in marine biodiversity. Based on historical ichthyoplankton (fish eggs and juvenile) observational records and multiple physical predictors, the seven major ichthyoplankton species in the YRE are projected to respond differently to environmental changes under the SSP 5·8·5 scenario^{219,220}: the distribution of *Coilia mystus* is projected to expand, whereas the distributions of the other six species shrink and shift northward (Supplementary Fig. 4).

Summary and future perspectives

Progress has been made in understanding how the physical, chemical and biological properties of the SAC have changed, and might continue to change, under a warming climate (Fig. 7). Substantial and accelerating surface warming trends have been observed in most parts of the SAC since the 1980s. This warming trend has led to more frequent and more intense MHWs, amplifying climate stress on marine ecosystems. Eutrophication induced by the input of terrestrial nutrients, along with warming-induced stratification, has further increased the severity of hypoxia and acidification in coastal waters, also affecting carbon storage through biological carbon pumps. Warming and nutrient changes, in turn, have caused a northward invasion of warm-water species and miniaturization, as robustly identified in plankton, benthos and fish, reflecting the reconfiguration of biological communities across the SAC. These biological changes have fundamentally affected the capacity of marine ecosystems to deliver services. These observed changes

are projected to persist or further amplify in the future. Yet, despite knowledge of these observed and projected changes, uncertainties and unknowns remain, as are now discussed.

Coastal and subsurface warming

Although knowledge of warming trends in the SAC is robust, there are gaps in understanding. A reliable quantification of SST increases in coastal waters, such as the BS, remains lacking, although coastal waters harbour most of the mariculture and contribute fundamentally to the total marine productivity of the SAC. Moreover, most existing assessments have focused on SST, with knowledge of subsurface waters, particularly the bottom layer, remaining fragmented. Yet warming in these deeper layers is pivotal in altering stratification and thereby hypoxia, acidification and marine productivity, limiting understanding in this regard. Therefore, observation-based datasets covering coastal and subsurface waters are needed. Given the sparse historical data sampling, deep-learning-based information mining techniques²²¹, in conjunction with satellite and model-based data, are expected to aid the generation of such datasets.

Circulation and surface heat fluxes

Downward heat fluxes from the atmosphere and horizontal heat advection by ocean circulation – two factors primarily controlling SAC warming – are poorly understood. Observed circulation changes are highly uncertain owing to natural variability (at interannual to interdecadal timescales) in monsoonal and Pacific winds that govern the Kuroshio and SAC circulation. Climate models – with refined resolution and topography to realistically represent the dynamics in the SAC – could

provide insights into climate-driven changes in circulation. Synchronous measurements of the sea surface and the atmospheric boundary layer properties, which are required in estimating surface heat fluxes through parameterizations^{222,223}, were in shortage in the SAC. Field campaigns have been conducted since 2010 in the SCS to support heat flux estimates²²⁴. Uncertainties are still too large to allow the identification of long-term changes²²⁵. Sustained measurements, possibly through arrays of moored buoys, and enhanced research efforts on parameterization schemes are required to reduce these uncertainties.

Compound stressors

Compound stressors (such as warming plus acidification²²⁶, warming plus sea-level rise²²⁷, or acidification plus hypoxia²²⁸) can exert more substantial biological impacts than the linear summation of individual impacts. Hypoxia and acidification often co-occur and operate synergistically to affect biosystems (particularly benthos) and have a range of ecological and socioeconomic impacts²²⁸. Compound stressors are expected to arise from extreme events such as MHWs. So far, the biological impacts of MHWs in the SAC remain underreported, which makes it difficult to mitigate the adverse consequences of future extreme events. Individual stressors and their synergistic impacts in such extreme events must be investigated, ideally through targeted in situ observation and regional modelling.

Prediction models for marine biodiversity

Given the ecological changes in the SAC, there is a pressing need to improve prediction models for marine biodiversity under climate change. At present, the widely adopted approach for biodiversity prediction is the regression of species biomass onto the projected seawater temperatures by climate models^{219,220,229,230}. Although bio-climate envelope models have a promising future in the projection of species distributions²²⁹, they are susceptible to model assumptions and data uncertainties²³¹, including the lack of biotic interactions, species dispersal, and the assumption that the observed species distributions are in equilibrium with the environment^{231,232}. Therefore, there is an urgent need to move toward more robust, holistic and ecologically realistic model experiments that incorporate interactions between stressors, as well as scaling up from individuals and populations to communities and ecosystems²³³. New generic dynamic bioclimate envelope models that incorporate population and dispersal dynamics of marine organisms offer an opportunity to achieve these objectives. They can provide more reliable projections of the shift rate of marine species distributions, local extinction, invasion and the combined effects on species turnover; reveal the potential hotspots of climate change impacts on marine biodiversity; and support the development of strategies to protect marine biodiversity and the formulation of laws and regulations.

Data availability

All the data used in this review are publicly available. The OISST data are available at <https://www.ncdc.noaa.gov/oisst>. The HadISST data are available at <https://climatedataguide.ucar.edu/climate-data/sst-data-hadisst-v1?qt-climatedatasetmain&tabs=4>. The COBE SST version-2 data are available at https://ds.data.jma.go.jp/gmd/goos/data/rrtadb/jma-pro/cobe2_sst_glb_M.html. The ERSST version-5 data are available at <https://climatedataguide.ucar.edu/climate-data/sst-data-noaa-extended-reconstruction-ssts-version-5-ersstv5>. MODIS Chl-a concentration data are available at https://modis.gsfc.nasa.gov/data/dataprod/chlor_a.php. CMIP6 simulations and projections are available

at <https://esgf-node.llnl.gov/projects/cmip6/>. Fisheries-related data are available at www.searoundus.org.

Published online: 18 July 2023

References

1. Pauly, D. et al. Sea Around Us concepts, design and data. <https://www.searoundus.org> (2020).
2. Wang, G. et al. Tropical cyclone genesis over the South China Sea. *J. Mar. Sys.* **68**, 318–326 (2007).
3. Ishii, M. et al. Objective analyses of sea-surface temperature and marine meteorological variables for the 20th century using ICOADS and the KOBE collection. *Int. J. Climatol.* **25**, 865–879 (2005).
4. Wang, F. et al. The long-term variability of sea surface temperature in the seas east of China in the past 40a. *Acta Oceanol. Sin.* **32**, 48–53 (2013).
5. Bao, B. & Ren, G. Climatological characteristics and long-term change of SST over the marginal seas of China. *Cont. Shelf Res.* **77**, 96–106 (2014).
6. Cai, R. et al. Robust surface warming in offshore china seas and its relationship to the East Asian monsoon wind field and ocean forcing on interdecadal time scales. *J. Clim.* **30**, 8987–9005 (2017).
7. Wu, L. et al. Enhanced warming over the global subtropical western boundary currents. *Nat. Clim. Change* **2**, 161–166 (2012).
8. Wu, C.-R. et al. Intrusion of the Kuroshio into the South and East China Seas. *Sci. Rep.* **7**, 7895 (2017).
9. Wei, Y. et al. Interannual to decadal variability of the Kuroshio current in the East China Sea from 1955 to 2010 as indicated by in-situ hydrographic data. *J. Oceanogr.* **69**, 571–589 (2013).
10. Huang, T.-H. et al. East China Sea increasingly gains limiting nutrient P from South China Sea. *Sci. Rep.* **9**, 5648 (2019).
11. Wei, Q. et al. Spatiotemporal variations in the summer hypoxia in the Bohai Sea (China) and controlling mechanisms. *Mar. Pollut. Bull.* **138**, 125–134 (2019).
12. Chi, L. et al. Distribution and key influential factors of dissolved oxygen off the Changjiang River estuary (CRE) and its adjacent waters in China. *Mar. Pollut. Bull.* **125**, 440–450 (2017).
13. Li, X.-L., Shi, H.-M., Xia, H.-Y., Zhou, Y.-P. & Qiu, Y.-W. Seasonal hypoxia and its potential forming mechanisms in the Mirs Bay, the northern South China Sea. *Cont. Shelf Res.* **80**, 1–7 (2014).
14. Cai, Y. et al. Stock distribution of a new record species *Nemipterus mesopion* in offshore northern South China Sea [in Chinese]. *South China Fish. Sci.* **16**, 516–519 (2020).
15. Jiao, N. et al. Carbon pools and fluxes in the China Seas and adjacent oceans. *Sci. China Earth Sci.* **61**, 1535–1563 (2018).
16. Jiao, N. et al. Deploying ocean negative carbon emissions to implement the carbon neutrality strategy [in Chinese]. *Sci. Sin. Terra* **51**, 632–643 (2021).
17. Wang, F. et al. Blue carbon sink function of Chinese coastal wetlands and carbon neutrality strategy [in Chinese]. *Bull. Chin. Acad. Sci.* **36**, 241–251 (2021).
18. Cai, R., Tan, H. & Qi, Q. Impacts of and adaptation to inter-decadal marine climate change in coastal China seas. *Int. J. Climatol.* **36**, 3770–3780 (2016).
19. Tang, S.-M. et al. Response of phytoplankton in offshore China seas to climate change [in Chinese]. *J. Appl. Oceanogr.* **36**, 455–465 (2017).
20. Li, X.-X. et al. Study on spatiotemporal changes of net primary productivity in Bohai Sea using MODIS data [in Chinese]. *Ecol. Environ. Sci.* **26**, 785–793 (2017).
21. Luan, Q.-S. et al. Long-term changes within the phytoplankton community in the Yellow Sea (1985–2015) [in Chinese]. *J. Fish. Sci. China* **27**, 1–11 (2020).
22. Yang, Q. et al. Zooplankton diversity and its variation in the northern Yellow Sea in the autumn and winter of 1959, 1982 and 2009. *Acta Ecol. Sin.* **32**, 6747–6754 (2012).
23. Xu, Z.-L. & Zhang, D. Dramatic declines in *Euphausia pacifica* abundance in the East China sea: response to recent regional climate change. *Zool. Sci.* **31**, 135–142 (2014).
24. Chen, B. et al. Impacts of climate changes on marine biodiversity [in Chinese]. *J. Oceanogr. Taiw. Strait* **28**, 437–444 (2009).
25. Wu, Z. et al. The long-term spatiotemporal variability of sea surface temperature in the northwest Pacific and China offshore. *Ocean. Sci.* **16**, 83–97 (2020).
26. Gao, G. et al. Drivers of marine heatwaves in the East China Sea and the South Yellow sea in three consecutive summers during 2016–2018. *J. Geophys. Res. Oceans* **125**, e2020JC016518 (2020).
27. Yao, Y. & Wang, C. Variations in summer marine heatwaves in the South China Sea. *J. Geophys. Res. Oceans* **126**, e2021JC017792 (2021).
28. Choi, W. et al. Characteristics and mechanisms of marine heatwaves in the East Asian marginal seas: regional and seasonal differences. *Remote Sens.* **14**, 3522 (2022).
29. Yao, Y. et al. Marine heatwaves in China's marginal seas and adjacent offshore waters: past, present, and future. *J. Geophys. Res. Oceans* **125**, e2019JC015801 (2020).
30. Li, L. et al. Behavior of arsenic in the coastal area of the Changjiang (Yangtze River) estuary: influences of water mass mixing, the spring bloom and hypoxia. *Cont. Shelf Res.* **80**, 67–78 (2014).
31. Chen, C.-C. et al. Hypoxia in autumn of the East China Sea. *Mar. Pollut. Bull.* **152**, 110875 (2020).
32. Jiang, Z. B. et al. Responses of summer phytoplankton community to drastic environmental changes in the Changjiang (Yangtze River) estuary during the past 50 years. *Water Res.* **54**, 1–11 (2014).

33. Kang, B. et al. Climate change impacts on China's marine ecosystems. *Rev. Fish Biol. Fish.* **31**, 599–629 (2021).
34. Zhang, J. et al. A comparative study on the macrobenthic community over a half century in the Yellow Sea, China. *J. Oceanogr.* **72**, 189–205 (2016).
35. Xu, Y. et al. Temporal variation of macrobenthic community zonation over nearly 60 years and the effects of latitude and depth in the southern Yellow Sea and East China Sea. *Sci. Total Environ.* **739**, 139760 (2020).
36. Zhang, X. et al. Potential influence of sea surface temperature on the interannual fluctuation of the catch and the distribution of chub mackerel and round scad in the Minnan-Taiwan Bank fishing ground, China [in Chinese]. *Mar. Sci. Bull.* **24**, 91–96 (2005).
37. Liang, C. et al. Impacts of ocean warming on China's fisheries catches: an application of 'mean temperature of the catch' concept. *Front. Mar. Sci.* **5**, 26 (2018).
38. Singh, T. et al. Effects of moderate thermal anomalies on Acropora corals around Sesoko Island, Okinawa. *PLoS ONE* **14**, e0210795 (2019).
39. Smith, K. E. et al. Socioeconomic impacts of marine heatwaves: global issues and opportunities. *Science* **374**, eabj3593 (2021).
40. Hansen, J. et al. Global surface temperature change. *Rev. Geophys.* **48**, RG4004 (2010).
41. Burrows, M. T. et al. The pace of shifting climate in marine and terrestrial ecosystems. *Science* **334**, 652–655 (2011).
42. Lima, F. P. & Wethay, D. S. Three decades of high-resolution coastal sea surface temperatures reveal more than warming. *Nat. Commun.* **3**, 704 (2012).
43. Zhang, L. et al. Modes and mechanisms of sea surface temperature low-frequency variations over the coastal China seas. *J. Geophys. Res.* **115**, C08031 (2010).
44. Rayner, N. A. et al. Global analyses of sea surface temperature, sea ice, and night marine air temperature since the late nineteenth century. *J. Geophys. Res. Oceans* **108**, 4407 (2003).
45. Trenberth, K. E. & Fasullo, J. T. An apparent hiatus in global warming? *Earth's Future* **1**, 19–32 (2013).
46. Kosaka, Y. & Xie, S.-P. Recent global-warming hiatus tied to equatorial Pacific surface cooling. *Nature* **501**, 403–407 (2013).
47. Mantua, N. J. et al. A Pacific interdecadal climate oscillation with impacts on salmon production. *Bull. Am. Meteorol. Soc.* **78**, 1069–1079 (1997).
48. Yeh, S.-W. & Kim, C.-H. Recent warming in the Yellow/East China Sea during winter and the associated atmospheric circulation. *Cont. Shelf Res.* **30**, 1428–1434 (2010).
49. Tang, Y. et al. Surface warming reacceleration in offshore China and its interdecadal effects on the East Asia-Pacific climate. *Sci. Rep.* **10**, 14811 (2020).
50. Yoon, J. & Yeh, S. W. Influence of the Pacific decadal oscillation on the relationship between El Niño and the northeast Asian summer monsoon. *J. Clim.* **23**, 4525–4537 (2010).
51. Kim, J. W. et al. Combined effect of El Niño–Southern Oscillation and Pacific Decadal Oscillation on the East Asian winter monsoon. *Clim. Dyn.* **42**, 957–971 (2014).
52. Andres, M. et al. Manifestation of the Pacific Decadal Oscillation in the Kuroshio. *Geophys. Res. Lett.* **36**, L16602 (2009).
53. Wang, Y. et al. Upper-ocean temperature trends in the Eastern China Seas during 1976–1996. *J. Oceanol. Limnol.* **36**, 1527–1536 (2018).
54. Oey, L.-Y. et al. Decadal warming of coastal China Seas and coupling with winter monsoon and currents. *Geophys. Res. Lett.* **40**, 6288–6292 (2013).
55. Sun, C. et al. Western tropical Pacific multidecadal variability forced by the Atlantic multidecadal oscillation. *Nat. Commun.* **8**, 15998 (2017).
56. Guo, Y. et al. Interannual to interdecadal variability of the Southern Yellow Sea cold water mass and establishment of 'forcing mechanism bridge'. *J. Mar. Sci. Eng.* **9**, 1316 (2021).
57. Park, K.-A. et al. Spatial and temporal variability of sea surface temperature and warming trends in the Yellow Sea. *J. Mar. Syst.* **143**, 24–38 (2015).
58. Sasaki, Y. N. & Umeda, C. Rapid warming of sea surface temperature along the Kuroshio and the China coast in the East China Sea during the 20th century. *J. Clim.* **34**, 4803–4815 (2021).
59. Tang, X. et al. Warming trend in northern East China Sea in recent four decades. *Chin. J. Oceanol. Limnol.* **27**, 185–191 (2009).
60. Li, Y. et al. Homogenization and trend analysis of 1960–2015 in situ sea surface temperature observations along the coast of China. *Acta Oceanol. Sin.* **40**, 36–46 (2021).
61. Li, A. et al. Long-term temperature variation of the Southern Yellow Sea cold water mass from 1976 to 2006. *Chin. J. Oceanol. Limnol.* **35**, 1032–1044 (2017).
62. Li, A. et al. Long-term variation in the salinity of the Southern Yellow Sea cold water mass, 1976–2006. *J. Oceanogr.* **73**, 321–331 (2017).
63. Hobday, A. J. et al. A hierarchical approach to defining marine heatwaves. *Prog. Oceanogr.* **141**, 227–238 (2016).
64. Liao, E. et al. The coastal ocean response to the global warming acceleration and hiatus. *Sci. Rep.* **5**, 16630 (2015).
65. Yan, Y. et al. Record-breaking sea surface temperatures in the Yellow and East China Seas. *J. Geophys. Res. Oceans* **125**, e2019JC015883 (2020).
66. Tan, H.-J. et al. Summer marine heatwaves in the South China Sea: trend, variability and possible causes. *Adv. Clim. Chang. Res.* **13**, 323–332 (2022).
67. Li, Y. et al. The 2016 record-breaking marine heatwave in the Yellow Sea and associated atmospheric circulation anomalies. *Atmos. Res.* **268**, 106011 (2022).
68. Wang, Q. et al. Properties and drivers of marine heat waves in the Northern South China Sea. *J. Phys. Oceanogr.* **52**, 917–927 (2022).
69. Chen, Y. et al. Extreme 2020 summer SSTs in the northern South China Sea: implications for the Beibu Gulf coral bleaching. *J. Clim.* **35**, 1–45 (2022).
70. Gordon, A. L. et al. The nascent Kuroshio of Lamon Bay. *J. Geophys. Res. Oceans* **119**, 4251–4263 (2014).
71. Nitani, H. in *Kuroshio: Its Physical Aspects*, 129–163 (Univ. Tokyo Press, 1972).
72. Duan, J. et al. Multidecadal change of the Mindanao Current: is there a robust trend? *Geophys. Res. Lett.* **46**, 6755–6764 (2019).
73. Zhai, F. et al. Decadal variations of the North Equatorial Current in the Pacific at 137°E. *J. Geophys. Res. Oceans* **118**, 4989–5006 (2013).
74. Chen, Z. & Wu, L. Long-term change of the Pacific North Equatorial Current bifurcation in SODA. *J. Geophys. Res. Oceans* **117**, C06016 (2012).
75. Hu, D. et al. Pacific western boundary currents and their roles in climate. *Nature* **522**, 299–308 (2015).
76. Nan, F. et al. Weakening of the Kuroshio intrusion into the South China Sea over the past two decades. *J. Clim.* **26**, 8097–8110 (2013).
77. Wu, C.-R. et al. Weakening of the Kuroshio intrusion into the South China Sea under the global warming hiatus. *IEEE J. Sel. Top. Appl. Earth Obs. Remote. Sens.* **9**, 5064–5070 (2016).
78. England, M. H. et al. Recent intensification of wind-driven circulation in the Pacific and the ongoing warming hiatus. *Nat. Clim. Change.* **4**, 222–227 (2014).
79. Qiu, B. & Chen, S. Multidecadal sea level and gyre circulation variability in the Northwestern Tropical Pacific Ocean. *J. Phys. Oceanogr.* **42**, 193–206 (2012).
80. Chang, Y. et al. Decreasing trend of Kuroshio intrusion and its effect on the chlorophyll-a concentration in the Luzon Strait, South China Sea. *Gisci. Remote Sens.* **59**, 633–647 (2022).
81. Sheremet, V. A. Hysteresis of a western boundary current leaping across a gap. *J. Phys. Oceanogr.* **31**, 1247–1259 (2001).
82. Zhou, C. et al. Increasing deep-water overflow from the Pacific into the South China Sea revealed by mooring observations. *Nat. Commun.* **14**, 2013 (2023).
83. Zhu, Y. et al. Weakening trend of Luzon Strait overflow transport in the past two decades. *Geophys. Res. Lett.* **49**, e2021GL097395 (2022a).
84. Hsin, Y.-C. Multidecadal variations of the surface Kuroshio between 1950s and 2000s and its impacts on surrounding waters. *J. Geophys. Res. Oceans* **120**, 1792–1808 (2015).
85. Wang, Y.-L. & Wu, C.-R. Discordant multi-decadal trend in the intensity of the Kuroshio along its path during 1993–2013. *Sci. Rep.* **8**, 14633 (2018).
86. Hsin, Y. C. et al. Seasonal to interannual variations in the intensity and central position of the surface Kuroshio east of Taiwan. *J. Geophys. Res. Oceans* **118**, 4305–4316 (2013).
87. Liu, Z. J. et al. Comprehensive observational features for the Kuroshio transport decreasing trend during a recent global warming hiatus. *Geophys. Res. Lett.* **48**, e2021GL094169 (2021).
88. Yang, H. & Wu, L. Trends of upper-layer circulation in the South China Sea during 1959–2008. *J. Geophys. Res. Oceans* **117**, C08037 (2012).
89. Zhu, Y. et al. Decadal weakening of abyssal South China Sea circulation. *Geophys. Res. Lett.* **49**, e2022GL100582 (2022b).
90. Zhang, C. et al. Enhancement of Zhe-Min coastal water in the Taiwan Strait in winter. *J. Oceanogr.* **76**, 197–209 (2020).
91. Jeong, J.-H. et al. Recent recovery of the Siberian high intensity. *J. Geophys. Res.* **116**, D23102 (2011).
92. Kim, Y.-S., Jang, C.-J. & Yeh, S.-W. Recent surface cooling in the Yellow and East China Seas and the associated North Pacific climate regime shift. *Cont. Shelf Res.* **156**, 43–54 (2018).
93. Wang, Y. et al. Evolution of satellite derived chlorophyll-a trends in the Bohai and Yellow Seas during 2002–2018: comparison between linear and nonlinear trends. *Estuar. Coast. Shelf Sci.* **259**, 107449 (2021).
94. Kim, I.-N. et al. Increasing anthropogenic nitrogen in the North Pacific Ocean. *Science* **346**, 1102–1106 (2014).
95. Wang, J. et al. Long-term nutrient variations in the Bohai Sea over the past 40 years. *J. Geophys. Res. Oceans* **124**, 703–722 (2019).
96. Zheng, L. & Zhai, W. Excess nitrogen in the Bohai and Yellow Seas, China: distribution, trends, and source apportionment. *Sci. Total Environ.* **794**, 148702 (2021).
97. Moon, J.-Y. et al. Anthropogenic nitrogen is changing the East China and Yellow Seas from being N deficient to being P deficient. *Limnol. Oceanogr.* **66**, 914–924 (2021).
98. Malone, T. C. & Newton, A. The globalization of cultural eutrophication in the coastal ocean: causes and consequences. *Front. Mar. Sci.* **7**, 670 (2020).
99. Zhang, J. et al. From the water sources of the Tibetan Plateau to the ocean: state of nutrients in the Changjiang linked to land use changes and climate variability. *Sci. China Earth Sci.* **65**, 2127–2174 (2022).
100. Kim, T.-W. et al. Increasing N abundance in the Northwestern Pacific ocean due to atmospheric nitrogen deposition. *Science* **334**, 505–509 (2011).
101. Liu, N. Review on the nutrients transport in Yangtze River with responses to the damming in the drainage basin in the past 50 years. *Environ. Chem.* **36**, 1579–1587 (2017).
102. Niu, L. et al. Impact of anthropogenic forcing on the environmental controls of phytoplankton dynamics between 1974 and 2017 in the Pearl River estuary, China. *Ecol. Indic.* **116**, 106484 (2020).
103. Wei, Q. et al. Long-term variation of nutrients in the southern Yellow Sea. *Cont. Shelf Res.* **111**, 184–196 (2015).
104. Hu, Y. et al. Interannual variation of nutrients along a transect across the Kuroshio and shelf area in the East China Sea over 40 years. *J. Oceanol. Limnol.* **36**, 62–76 (2018).
105. Du, C. et al. Impact of the Kuroshio intrusion on the nutrient inventory in the upper northern South China Sea: insights from an isopycnal mixing model. *Biogeosciences* **10**, 6419–6432 (2013).

106. Yang, F. et al. Long-term variations and influence factors of nutrients in the western North Yellow Sea, China. *Mar. Pollut. Bull.* **135**, 1026–1034 (2018).
107. Li, H. et al. Changes in concentrations of oxygen, dissolved nitrogen, phosphate, and silicate in the southern Yellow Sea, 1980–2012: sources and seaward gradients. *Estuar. Coast. Shelf Sci.* **163**, 44–55 (2015).
108. Lin, C. et al. Environmental changes and the responses of the ecosystems of the Yellow Sea during 1976–2000. *J. Mar. Syst.* **55**, 223–234 (2005).
109. Ning, X. et al. Long term changes in the ecosystem in the northern South China Sea during 1976–2004. *Biogeosciences* **6**, 2227–2243 (2009).
110. Xin, M. et al. Long-term changes in nutrient regimes and their ecological effects in the Bohai Sea, China. *Mar. Pollut. Bull.* **146**, 562–573 (2019).
111. Zhang, H. et al. Contribution of sediment oxygen demand to hypoxia development off the Changjiang estuary. *Estuar. Coast. Shelf Sci.* **192**, 149–157 (2017).
112. Chi, L. et al. Main factors dominating the development, formation and dissipation of hypoxia off the Changjiang estuary (CE) and its adjacent waters, China. *Environ. Pollut.* **265**, 115066 (2020).
113. Li, Z. et al. The sinking of the phytoplankton community and its contribution to seasonal hypoxia in the Changjiang (Yangtze River) estuary and its adjacent waters. *Estuar. Coast. Shelf Sci.* **208**, 170–179 (2018).
114. Wang, H. et al. Eutrophication-driven hypoxia in the East China Sea off the Changjiang estuary. *Environ. Sci. Technol.* **50**, 2255–2263 (2016).
115. Chi, L. et al. Heterogeneity of the sediment oxygen demand and its contribution to the hypoxia off the Changjiang estuary and its adjacent waters. *Mar. Pollut. Bull.* **172**, 112920 (2022).
116. Wei, Q. et al. Mechanisms leading to the frequent occurrences of hypoxia and a preliminary analysis of the associated acidification off the Changjiang estuary in summer. *Sci. China Earth Sci.* **60**, 360–381 (2017).
117. Chen, X. et al. Tidal modulation of the hypoxia adjacent to the Yangtze estuary in summer. *Mar. Pollut. Bull.* **100**, 453–463 (2015).
118. Wei, X. et al. A model study of the effects of river discharges and winds on hypoxia in summer in the Pearl River estuary. *Mar. Pollut. Bull.* **113**, 414–427 (2016).
119. Guo, X. et al. Does submarine groundwater discharge contribute to summer hypoxia in the Changjiang (Yangtze) River estuary? *Sci. Total Environ.* **719**, 137450 (2020).
120. Guo, J. et al. Hypoxia, acidification and nutrient accumulation in the Yellow Sea Cold Water of the South Yellow Sea. *Sci. Total Environ.* **745**, 141050 (2020).
121. Li, X. et al. Deep-learning-based information mining from ocean remote-sensing imagery. *Natl Sci. Rev.* **7**, 1584–1605 (2020).
122. Li, C. et al. Effects of warming, eutrophication and climate variability on acidification of the seasonally stratified North Yellow Sea over the past 40 years. *Sci. Total Environ.* **815**, 152935 (2022).
123. Qian, W. et al. Current status of emerging hypoxia in a eutrophic estuary: the lower reach of the Pearl River estuary, China. *Estuar. Coast. Shelf Sci.* **205**, 58–67 (2018).
124. Ni, X. et al. The impact of wind mixing on the variation of bottom dissolved oxygen off the Changjiang estuary during summer. *J. Mar. Syst.* **154**, 122–130 (2016).
125. Wang, B. et al. Annual cycle of hypoxia off the Changjiang (Yangtze River) estuary. *Mar. Environ. Res.* **77**, 1–5 (2012).
126. Wu, Y. et al. Increasing hypoxia in the Changjiang estuary during the last three decades deciphered from sedimentary redox-sensitive elements. *Mar. Geol.* **419**, 106044 (2020).
127. Zhao, J. et al. Sedimentary organic and inorganic records of eutrophication and hypoxia in and off the Changjiang estuary over the last century. *Mar. Pollut. Bull.* **99**, 76–84 (2015).
128. Yang, J. et al. Sedimentary processes dominate nitrous oxide production and emission in the hypoxic zone off the Changjiang River estuary. *Sci. Total Environ.* **827**, 154042 (2022).
129. Liu, J. et al. Sedimentary phosphorus cycling and budget in the seasonally hypoxic coastal area of Changjiang estuary. *Sci. Total Environ.* **713**, 136389 (2020).
130. Zhai, W. Exploring seasonal acidification in the Yellow Sea. *Sci. China Earth Sci.* **61**, 647–658 (2018).
131. Wu, L. et al. Dissolved oxygen distributions, hypoxic and acidification characteristics, and their controlling factors in the southern Yellow Sea and off the Changjiang estuary. *Chin. Environ. Sci.* **41**, 1311–1324 (2021).
132. Shi, Q. et al. Acidification process of Bohai Sea water in recent 36 years. *Excellent Proceedings on Puhua Environmental Protection, Academic Annual Meeting of Chinese Society for Environmental Sciences 59–66* (Chinese Society for Environmental Sciences, Beijing, 2013).
133. Liu, X. et al. Acidification and the factors in surface seawater of the East China Sea coast. *Oceanol. Limnol. Sin.* **48**, 398–405 (2017).
134. Yang, X. et al. Treated wastewater changes the export of dissolved inorganic carbon and its isotopic composition and leads to acidification in coastal oceans. *Environ. Sci. Technol.* **52**, 5590–5599 (2018).
135. Xue, L. et al. Processes controlling sea surface pH and aragonite saturation state in a large northern temperate bay: contrasting temperature effects. *J. Geophys. Res. Biogeosci.* **125**, e2020JG005805 (2020).
136. Zhang, J. & Gao, X. Nutrient distribution and structure affect the acidification of eutrophic ocean margins: a case study in southwestern coast of the Laizhou Bay, China. *Mar. Pollut. Bull.* **111**, 295–304 (2016).
137. Liu, Q. et al. Carbon fluxes in the China Seas: an overview and perspective. *Sci. China Earth Sci.* **61**, 1564–1582 (2018).
138. Liu, Q. et al. Partial pressure of CO₂ and air-sea CO₂ fluxes in the South China Sea: synthesis of an 18-year dataset. *Prog. Oceanogr.* **182**, 102272 (2020).
139. Zhai, W. et al. Seasonal variations of sea-air CO₂ fluxes in the largest tropical marginal sea (South China Sea) based on multiple-year underway measurements. *Biogeosciences* **10**, 7775–7791 (2013).
140. Cai, R. & Chen, X. A changing ocean and its impact on climate change in China. *Resour. Environ.* **30**, 9–20 (2020).
141. Cai, W. Estuarine and coastal ocean carbon paradox: CO₂ sinks or sites of terrestrial carbon incineration? *Annu. Rev. Mar. Sci.* **3**, 123–145 (2011).
142. Bauer, J. E. et al. The changing carbon cycle of the coastal ocean. *Nature* **504**, 61–70 (2013).
143. Riebesell, U. et al. Sensitivities of marine carbon fluxes to ocean change. *Proc. Natl Acad. Sci. USA* **106**, 20602–20609 (2009).
144. Lønborg, C. et al. Impacts of global change on ocean dissolved organic carbon (DOC) cycling. *Front. Mar. Sci.* **7**, 466 (2020).
145. Dai, M. et al. Carbon fluxes in the coastal ocean: synthesis, boundary processes, and future trends. *Annu. Rev. Earth Planet. Sci.* **50**, 593–626 (2022).
146. Henson, S. A. et al. Detection of anthropogenic climate change in satellite records of ocean chlorophyll and productivity. *Biogeosciences* **7**, 621–640 (2010).
147. O'Reilly, J. E. & Werdell, P. J. Chlorophyll algorithms for ocean color sensors — OC4, OC5 & OC6. *Remote. Sens. Environ.* **229**, 32–47 (2019).
148. Qiao, Y. et al. Long-term changes in nutrients, chlorophyll a and their relationships in a semi-enclosed eutrophic ecosystem, Bohai Bay, China. *Mar. Pollut. Bull.* **117**, 222–228 (2017).
149. Fu, M. et al. Changes of nutrient concentrations and N:P:Si ratios and their possible impacts on the Huanghai Sea ecosystem. *Acta Oceanol. Sin.* **31**, 101–112 (2012).
150. Syndeman, W. J. et al. Climate change and wind intensification in coastal upwelling ecosystems. *Science* **345**, 77–80 (2014).
151. Xiu, P. et al. Future changes in coastal upwelling ecosystems with global warming: the case of the California current system. *Sci. Rep.* **8**, 2866 (2018).
152. Yu, Y. et al. The variability of chlorophyll-a and its relationship with dynamic factors in the basin of the South China Sea. *J. Mar. Syst.* **200**, 103230 (2019).
153. Wang, Y. et al. Long-term nutrient variation trends and their potential impact on phytoplankton in the southern Yellow Sea, China. *Acta Oceanol. Sin.* **41**, 54–67 (2022).
154. Zhai, F. et al. Interannual-decadal variation in satellite-derived surface chlorophyll-a concentration in the Bohai Sea over the past 16 years. *J. Mar. Syst.* **215**, 103496 (2021).
155. Xiu, P. et al. On contributions by wind-induced mixing and eddy pumping to interannual chlorophyll variability during different ENSO phases in the northern South China Sea. *Limnol. Ocean.* **64**, 503–514 (2019).
156. Sun, X. et al. Long-term changes of phytoplankton community structure in the Jiaozhou Bay [in Chinese]. *Oceanol. Limnol. Sin.* **42**, 639–646 (2011).
157. Lin, G. & Yang, Q. Interdecadal variation in distribution features of phytoplankton in the Taiwan Strait under global climate change [in Chinese]. *Chin. J. Appl. Environ. Biol.* **17**, 615–623 (2011).
158. Jiang, Z. et al. Controlling factors of summer phytoplankton community in the Changjiang (Yangtze River) estuary and adjacent East China Sea shelf. *Cont. Shelf Res.* **101**, 71–84 (2015).
159. Li, H. et al. Distribution of dissolved inorganic nutrients and dissolved oxygen in the high frequency area of harmful alga blooms in the East China Sea in spring. *Environ. Sci.* **34**, 2159–2165 (2013).
160. Zhou, Y. et al. Nutrients structure changes impact the competition and succession between diatom and dinoflagellate in the East China Sea. *Sci. Total Environ.* **574**, 499–508 (2017).
161. Luan, Q. et al. Long-term changes in the phytoplankton community in the Bohai Sea (1959–2015) [in Chinese]. *Prog. Fish. Sci.* **39**, 9–18 (2018).
162. Litchman, E. et al. The role of functional traits and trade-offs in structuring phytoplankton communities: scaling from cellular to ecosystem level. *Ecol. Lett.* **10**, 1170–1181 (2007).
163. Sun, X. & Sun, S. Phytoplankton size structure and its temporal and spatial changes in Jiaozhou Bay [in Chinese]. *Oceanol. Limnol. Sin.* **43**, 411–418 (2012).
164. Li, T. et al. Phytoplankton size classes changed oppositely over shelf and basin areas of the South China Sea during 2003–2018. *Prog. Oceanogr.* **191**, 102496 (2021).
165. Kodama, T. et al. Environmental factors controlling zooplankton accumulation in the near-surface layer in the western North Pacific marginal seas. *J. Mar. Syst.* **237**, 103829 (2023).
166. Sun, S. et al. Changes in the small-jellyfish community in recent decades in Jiaozhou Bay, China. *J. Ocean. Limnol.* **30**, 12 (2012).
167. Wang, W. et al. Zooplankton community structure, abundance and biovolume in Jiaozhou Bay and the adjacent coastal Yellow Sea during summers of 2005–2012: relationships with increasing water temperature. *J. Oceanol. Limnol.* **36**, 1655–1670 (2018).
168. Xu, Y. et al. Relationships of interannual variability in SST and phytoplankton blooms with giant jellyfish (*Nemopilema nomurai*) outbreaks in the Yellow Sea and East China Sea. *J. Oceanogr.* **69**, 511–526 (2013).
169. Kitajima, S. et al. Temporal fluctuations in abundance and size of the giant jellyfish *Nemopilema nomurai medusae* in the northern East China Sea, 2006–2017. *Mar. Biol.* **167**, (2020).
170. Xing, Q. et al. The evolutions of the typical ecological hazards in the Bohai Sea. *Coast. Sci.* **4**, 11–18 (2017).
171. Yang, L. et al. Zooplankton community variation and its relationship with environmental variables in Bohai Bay. *J. Mar. Syst.* **36**, 93–101 (2018).

172. Garzke, J. et al. Climate change affects low trophic level marine consumers: warming decreases copepod size and abundance. *Oecologia* **177**, 849–860 (2014).
173. Turner, J. T. The importance of small planktonic copepods and their roles in pelagic marine food webs. *Zool. Stud.* **43**, 255–266 (2004).
174. Smale, D. A. et al. Marine heatwaves threaten global biodiversity and the provision of ecosystem services. *Nat. Clim. Change* **9**, 306–312 (2019).
175. Doney, S. C. et al. The impacts of ocean acidification on marine ecosystems and reliant human communities. *Annu. Rev. Environ. Resour.* **45**, 83–112 (2020).
176. Sampaio, E. et al. Impacts of hypoxic events surpass those of future ocean warming and acidification. *Nat. Ecol. Evol.* **5**, 311–321 (2021).
177. Riedel, B. et al. Effect of hypoxia and anoxia on invertebrate behaviour: ecological perspectives from species to community level. *Biogeosciences* **11**, 1491–1518 (2014).
178. Yasuda, T. et al. Fishing ground hotspots reveal long-term variation in chub mackerel *Scomber japonicus* habitat in the East China Sea. *Mar. Ecol. Prog. Ser.* **501**, 239–250 (2014).
179. Xu, Y. et al. Seasonal and spatial variations of macrobenthic community structure and diversity in the south Yellow Sea. *Aquat. Ecosyst. Health Manag.* **19**, 92–100 (2016).
180. Zhang, J. et al. What has happened to the benthic mollusks of the Yellow Sea in the near half century? Comparison on molluscan biodiversity between 1959 and 2007. *Cont. Shelf Res.* **113**, 21–29 (2016).
181. Hu, L. & Dong, Y. Northward shift of a biogeographical barrier on China's coast. *Divers. Distrib.* **28**, 318–330 (2022).
182. Wang, W. et al. Global warming and artificial shorelines reshape seashore biogeography. *Glob. Ecol. Biogeogr.* **29**, 220–231 (2020).
183. White, M. M. et al. Early exposure of bay scallops (*Argopecten irradians*) to high CO₂ causes a decrease in larval shell growth. *PLoS ONE* **8**, e61065 (2013).
184. Sui, Y. et al. Defense responses to short-term hypoxia and seawater acidification in the thick shell mussel *Mytilus coruscus*. *Front. Physiol.* **8**, 145 (2017).
185. Meng, Y. et al. Calcium carbonate unit realignment under acidification: a potential compensatory mechanism in an edible estuarine oyster. *Mar. Pollut. Bull.* **139**, 141–149 (2019).
186. Tomasetti, S. J. et al. Warming and hypoxia reduce the performance and survival of northern bay scallops (*Argopecten irradians irradians*) amid a fishery collapse. *Glob. Change Biol.* **29**, 2092–2107 (2023).
187. Zhai, W. et al. Coastal acidification in summer bottom oxygen-depleted waters in northwestern–northern Bohai Sea from June to August in 2011. *Chin. Sci. Bull.* **57**, 1062–1068 (2012).
188. Dahlke, F. T. et al. Thermal bottlenecks in the life cycle define climate vulnerability of fish. *Science* **369**, 65–70 (2020).
189. Asch, R. G. et al. Climate change impacts on mismatches between phytoplankton blooms and fish spawning phenology. *Glob. Change Biol.* **25**, 2544–2559 (2019).
190. Lindmark, M. et al. Temperature impacts on fish physiology and resource abundance lead to faster growth but smaller fish sizes and yields under warming. *Glob. Change Biol.* **28**, 6239–6253 (2022).
191. Sherman, K. et al. Accelerated warming and emergent trends in fisheries biomass yields of the world's large marine ecosystems. *Ambio* **38**, 215–224 (2009).
192. Freitas, C. et al. Sea temperature effects on depth use and habitat selection in a marine fish community. *J. Anim. Ecol.* **90**, 1787–1800 (2021).
193. Free, C. M. et al. Impacts of historical warming on marine fisheries production. *Science* **363**, 979–983 (2019).
194. Chen, C. Chemical and physical fronts in the Bohai, Yellow and East China Seas. *J. Mar. Syst.* **78**, 394–410 (2009).
195. Hu, W. et al. Effects of climate change in the seas of China: predicted changes in the distribution of fish species and diversity. *Ecol. Indic.* **134**, 108489 (2022).
196. Cheung, W. W. L. et al. Large-scale redistribution of maximum fisheries catch potential in the global ocean under climate change. *Glob. Change Biol.* **16**, 24–35 (2010).
197. Sumaila, U. R. et al. Climate change impacts on the biophysics and economics of world fisheries. *Nat. Clim. Change* **1**, 449–456 (2011).
198. Kang, B. et al. Fisheries in Chinese seas: what can we learn from controversial official fisheries statistics? *Rev. Fish Biol. Fish.* **28**, 503–519 (2018).
199. Du Pontavice, H. et al. Climate change undermines the global functioning of marine food webs. *Glob. Change Biol.* **26**, 1306–1318 (2020).
200. Eyring, V. et al. Overview of the Coupled Model Intercomparison Project phase 6 (CMIP6) experimental design and organization. *Geosci. Model Dev.* **9**, 1937–1958 (2016).
201. Song, C. et al. Evaluation and projection of SST in the China seas from CMIP5. *Acta Oceanol. Sin.* **38**, 1–11 (2016).
202. Tan, H. et al. Projections of changes in marine environment in coastal China seas over the 21st century based on CMIP5 models. *J. Oceanol. Limnol.* **38**, 1676–1691 (2020).
203. Yu, X. et al. Future projection of East China Sea temperature by dynamic downscaling of the IPCC AR4 CCSM3 model result. *Chin. J. Oceanol. Limnol.* **30**, 826–842 (2012).
204. Qiu, Z. et al. Evaluation and projection of global marine heatwaves based on CMIP6 models. *Deep. Sea Res. Part II Top. Stud. Oceanogr.* **194**, 104998 (2021).
205. Frölicher, T. L. et al. Marine heatwaves under global warming. *Nature* **560**, 360–364 (2018).
206. Chen, C. et al. Why does global warming weaken the Gulf Stream but intensify the Kuroshio? *J. Clim.* **32**, 7437–7451 (2019).
207. Yang, H. et al. Intensification and poleward shift of subtropical western boundary currents in a warming climate. *J. Geophys. Res. Oceans* **121**, 4928–4945 (2016).
208. Hu, S. et al. Deep-reaching acceleration of global mean ocean circulation over the past two decades. *Sci. Adv.* **6**, eaax7727 (2020).
209. Peng, Q. et al. Surface warming-induced global acceleration of upper ocean currents. *Sci. Adv.* **8**, eabj8394 (2022).
210. Hao, J. et al. Long-term changes of cross-shelf transports in the Yellow and East China Seas under different greenhouse gases emission scenarios. *Clim. Dyn.* **59**, 1451–1471 (2021).
211. Kieran, P. H. et al. Observed decreases in oxygen content of the global ocean. *Geophys. Res. Lett.* **38**, L23602 (2011).
212. Wang, M. et al. Global change can make coastal eutrophication control in China more difficult. *Earths Future* **8**, e2019EF001280 (2020).
213. Wang, J. et al. Harmful algal blooms in Chinese coastal waters will persist due to perturbed nutrient ratios. *Environ. Sci. Technol. Lett.* **8**, 276–284 (2021).
214. Strokis, M. et al. Increasing eutrophication in the coastal seas of China from 1970 to 2050. *Mar. Pollut. Bull.* **85**, 123–140 (2014).
215. Boyce, D. G. et al. Global phytoplankton decline over the past century. *Nature* **466**, 591–596 (2010).
216. Poloczanska, E. S. et al. Responses of marine organisms to climate change across oceans. *Front. Mar. Sci.* **3**, 62 (2016).
217. Chaudhary, C. et al. Global warming is causing a more pronounced dip in marine species richness around the Equator. *Proc. Natl. Acad. Sci. USA* **118**, e2015094118 (2021).
218. Xu, Y. et al. Potential effects of climate change on the habitat suitability of macrobenthos in the Yellow Sea and East China Sea. *Mar. Pollut. Bull.* **174**, 113238 (2022).
219. Zhang, Z. et al. Modelling the potential impacts of climate change on the distribution of ichthyoplankton in the Yangtze estuary, China. *Divers. Distrib.* **26**, 126–137 (2020).
220. Zhang, Z. et al. Does weight presence records improve the performance of species distribution models? A test using fish larval stages in the Yangtze estuary. *Sci. Total Environ.* **741**, 140393 (2020).
221. Li, X. et al. Deep learning-based information mining from ocean remote sensing imagery. *National Sci. Rev.* **7**, 1584–1605 (2020).
222. Song, X. The importance of relative wind speed in estimating air-sea turbulent heat fluxes in bulk formulas: examples in the Bohai Sea. *J. Atmos. Ocean. Technol.* **37**, 589–603 (2020).
223. Zhang, R. et al. Cool skin effect and its impact on the computation of the latent heat flux in the South China Sea. *J. Geophys. Res. Oceans* **126**, e2020JC016498 (2021).
224. Yang, L. et al. Toward a mesoscale hydrological and marine meteorological observation network in the South China Sea. *Bull. Am. Meteorol. Soc.* **96**, 1117–1135 (2015).
225. Wang, X. et al. Biases of five latent heat flux products and their impacts on mixed-layer temperature estimates in the South China Sea. *J. Geophys. Res. Oceans* **122**, 5088–5104 (2017).
226. Harvey, B. P. et al. Meta-analysis reveals complex marine biological responses to the interactive effects of ocean acidification and warming. *Ecol. Evol.* **3**, 2782–2782 (2013).
227. Han, W. et al. Sea level extremes and compounding marine heatwaves in coastal Indonesia. *Nat. Commun.* **13**, 6410 (2022).
228. Steckbauer, A. et al. Synergistic effects of hypoxia and increasing CO₂ on benthic invertebrates of the central Chilean coast. *Front. Mar. Sci.* **2**, 49 (2015).
229. Cheung, W. W. L. et al. Projecting global marine biodiversity impacts under climate change scenarios. *Fish Fish.* **10**, 235–251 (2009).
230. Ibarbalz, F. M. et al. Global trends in marine plankton diversity across kingdoms of life. *Cell* **179**, 1084–1097 (2009).
231. Pearson, R. G. & Dawson, T. P. Predicting the impacts of climate change on the distribution of species: are bioclimate envelope models useful? *Glob. Ecol. Biogeogr.* **12**, 361–371 (2003).
232. Guisan, A. & Thuiller, W. Predicting species distribution: offering more than simple habitat models. *Ecol. Lett.* **8**, 993–1009 (2005).
233. Harley, C. D. G. et al. The impacts of climate change in coastal marine systems. *Ecol. Lett.* **9**, 228–241 (2006).
234. Reynolds, R. W. et al. Daily high-resolution-blended analyses for sea surface temperature. *J. Clim.* **20**, 5473–5496 (2007).
235. Huang, B. et al. Extended Reconstructed Sea Surface Temperature version 5 (ERSSTv5), upgrades, validations, and intercomparisons. *J. Clim.* **30**, 8179–8205 (2017).
236. China's Ocean Survey Report (State Oceanic Administration, 1959).
237. Tian, R. et al. Summer nutrient fronts in the Changjiang (Yangtze River) Estuary. *Estuar. Coast. Shelf Sci.* **37**, 27–41 (1993).
238. Li, D. et al. Oxygen depletion off the Changjiang (Yangtze River) Estuary. *Sci. China Ser. D* **32**, 686–694 (2002).
239. Shi, J. et al. Bottom fine sediment boundary layer and transport processes at the mouth of the Changjiang Estuary, China. *J. Hydrol.* **327**, 276–288 (2006).
240. Chen, C. et al. Hypoxia in the East China Sea: one of the largest coastal low-oxygen areas in the world. *Mar. Environ. Res.* **64**, 399–408 (2008).
241. Zhang, Z. et al. Spatio-temporal variation, formation and transformation of the hypoxia area off the Yangtze River estuary. *Mar. Environ. Sci.* **31**, 469–473 (2012).
242. Liu, H. et al. Study on the variation trend and influencing factors of summer hypoxia off the Yangtze River estuary. *Mar. Environ. Sci.* **40**, 341–351 (2021).
243. Sun, S. et al. In *Processes and Changes of Aquatic Ecosystem* (ed. Qin, B.) 300–346 (Higher Education Press, 2019).
244. Wang, W. et al. Seasonal phenology of the heterotrophic dinoflagellate *Noctiluca scintillans* (Macartney) in Jiaozhou Bay and adjacent coastal Yellow Sea, China. *J. Oceanol. Limnol.* **36**, 1280–1293 (2018).

Acknowledgements

This work is supported by the Natural Science Foundation of China (42090040), the Strategic Priority Research Program of Chinese Academy of Sciences grant (XDB42000000) and the National Key R&D Program of China (2017YFA0603200). Y.L. is supported by Shandong Provincial Natural Science Foundation (ZR2020JQ17). H.Z. is supported by the National Key Research and Development Project of China (2022YFE0112800). J.Z. is supported by Intergovernmental International Cooperation in Science and Technology Innovation (2021YFE0193700).

Author contributions

All the authors contributed to writing and editing the article. F.W. and Y.L. led the overall concept design and coordinated the writing. X.T. and F.W. led the warming trend section. X.T. and Y.Y. led the marine heatwaves section. D.Y. and L.X. led the circulation changes section. X.L. led the nutrients, hypoxia and acidification sections. H.Y. led the carbon storage section. X.S. and Y.W. led the plankton section. J.Z. led the benthos section. H.Z. led the fishes and fishery resources section. Y.L. and X.T. led the projected changes section. F.W. and Y.L. led the summary and future perspectives section. Y.G. and Q.R. contributed to data processing and graphing. All authors contributed to writing and editing.

Competing interests

The authors declare no competing interests.

Additional information

Supplementary information The online version contains supplementary material available at <https://doi.org/10.1038/s43017-023-00453-6>.

Peer review information *Nature Reviews Earth & Environment* thanks Shuyang Ma, Kitack Lee and the other, anonymous, reviewer(s) for their contribution to the peer review of this work.

Publisher's note Springer Nature remains neutral with regard to jurisdictional claims in published maps and institutional affiliations.

Springer Nature or its licensor (e.g. a society or other partner) holds exclusive rights to this article under a publishing agreement with the author(s) or other rightsholder(s); author self-archiving of the accepted manuscript version of this article is solely governed by the terms of such publishing agreement and applicable law.

© Springer Nature Limited 2023